AD-A085 587 UNIVERSITY OF SOUTHERN CALIFORNIA LOS ANGELES DEPT O--ETC F/G 20/4
ANALYSIS OF TRANSONIC SWEPT WINGS USING ASYMPTOTIC AND OTHER NU--ETC(U)
MAY 80 H K CHENG, S Y MENG, R CHOW, R SMITH N00014-75-C-0520

UNCLASSIFIED USCAE-138 NL

END
DATE FILMED
7-80
DTIC

(14) USCAE-138
May 1980
(11)

(12) 30

(6) ANALYSIS OF TRANSONIC SWEPT WINGS USING ASYMPTOTIC AND OTHER NUMERICAL METHODS.

(9) Technical Rept.,

(10) H.K./Cheng, S.Y./Meng R./Chow R./Smith
Department of Aerospace Engineering
University of Southern California
Los Angeles, California

R. Chow
Grumman Aerospace Corporation
Bethpage, New York

R. Smith
NASA Ames Research Center
Moffett Field, California

DTIC
ELECTE
JUN 1 1980
D

Office of Naval Research
(15) Contract No. N00014-75-C-0520
Identification Number NR 061-192

This document has been approved for public release and sale; its distribution is unlimited.

4/02 017

FOREWARD

This paper was presented at the AIAA 18th Aerospace Sciences Meeting, held at Pasadena, California on January 14-16, 1980. The text has appeared as a preprint AIAA-80-0342. Since reprints of the work are unavailable, the paper, with up-dated errata sheets included, is distributed here as a University of Southern California School of Engineering, Department of Aerospace Engineering Report, USCAE 138.

The work presents a comparison of analyses based on the asymptotic theory for high aspect ratio wings with corresponding results from a 3-D full-potential computer code (FLO 22) for oblique wings as well as a more conventional swept wing involving highly subcritical and slightly supercritical component flows.

The paper also gives a survey and critique of the relatively recent developments in the lifting-line theory. The material presented obviously cannot be accomodated by the length of a single standard journal article; various parts of this work are not expected to reach journal publication stage for some time. The distribution of this report should therefore serve a useful purpose.

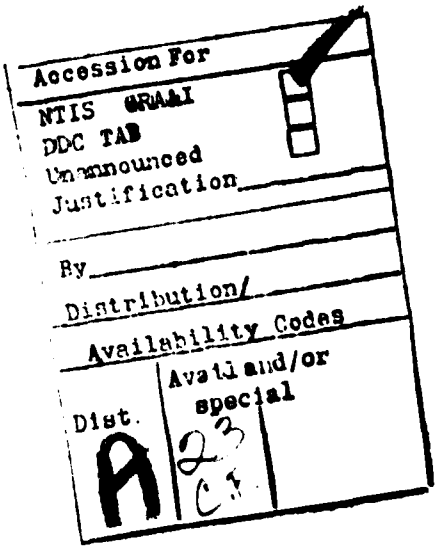

ERRATA

"TRANSONIC SWEPT-WING ANALYSES USING ASYMPTOTIC AND OTHER NUMERICAL METHODS"

(AIAA Paper 80-0342)

H.K. Cheng, S.Y. Meng, R. Chow and R. Smith

Page 1, left column, 17th line in Abstract, change "swept-forward-wing" to "swept-forward wing".

Page 1, right column, 15th line from bottom, insert "and" between "wings" and "conven-".

Page 1, right column 4th line from the bottom, change "analysis" to "analyses".

Page 2, left column, Eq. (2.1), change "M_n" to "M_∞".

Page 2, left column, 14th line from the bottom, replace "that" with "the scale".

Page 2, right column, end of second paragraph, change "(57)" to "(56)"; below Eq. (2.6b), change "where" to "while"; Eq. (2.6c), replace "m" with "$\bar{m}$".

Page 3, left and right columns, Section 2.2, Weissinger has been cited and misspelled four times.

Page 3, left column, 5th line below Eq. (2.7), add comma after "turn"; 7th line below Eq. (2.7), replace "(37)" by "(36)"; second line of § 2.2, move "28-30" to the front of the parenthesis.

Page 3, right column, 13th line of § 2.3, replace "(38)" with "(37)".

Page 4, left column, 24th line from the bottom, insert "will" between "but" and "reduce".

Page 6, right column, § 3.4, 2nd line from the top, change "admits" to "admit".

Page 6, right column, Eq. (3.11), replace "$\partial \hat{x}$" with "$\frac{\partial}{\partial \hat{x}}$".

Page 7, left column, § 3.5, 2nd line from the top, change "existance" to "existence".

Page 8, left column, 23rd line from the top, change "because" to "from".

Page 8, left column, footnote, replace "(53)" with "(52)".

Errata (continued)

Page 9, left column, § 4, 3rd line from the top, change "lead" to "leads".

Page 9, right column, 4th line from the top, change "posess" to "possess".

Page 11, left column, 7th line from the top, change "vorticities" to "vorticity".

Page 11, left column, 26th line from the top, change "30°" to "22.5°" and "M_∞ = .755" to "M_∞ = .824".

Page 11, left column, 39th line from the top, change "Futhermore" to "Furthermore"

Page 11, right column, 3rd line from the bottom, change "convergenced" to "converged".

Page 11, right column, 5th line of § 5.2, replace "(50)" with "(59)".

Page 12, left column, 2nd line of § 5.3 replace "(4.62)" with "(11,62)"; 3rd paragraph § 5.2, 4th line, add Ref. 22.

Page 13, left column, 2nd line from the end of § 5, change "is" to "based".

Page 13, left column, 30th line from the top, delete "is".

Page 13, left column, 22nd line from the bottom, change "vorticities" to "vorticity".

Page 13, right column, 5th line from the bottom, correct the author's name to read "Küchemann".

Page 13, right column, Reference 1: change "Buseman" to "Busemann"; write "Uberschallgesch Windigkeit" as a single word.

Page 13, right column, Reference 4: change "Kucheman" to "Kuchemann".

Page 14, left column, Reference 14a: change "to appear in...." to "Journal of Fluid Mechanics", Vol. 97, pt. 3, 1980, pp. 531-556".

Page 14, left column, Reference 19: write "Traflugel Theorie" as a single word.

Page 14, right column, Reference 28: change "Weisinger" to "Weissinger".

Page 15, right column, Reference 55: delete "and" from the 3rd line.

Page 15, right column, Reference 57: make the first letters in "Senkrechten", "Einer", and "Gekrummten" lower case.

Page 15, right column, the Caption of Fig. 1, 3rd line from the bottom, change "swept-wing" to "swept-wings".

Page 16, the Caption of Fig. 7, change "D" to lower "d".

TRANSONIC SWEPT-WING ANALYSIS USING ASYMPTOTIC AND OTHER NUMERICAL METHODS

H.K. Cheng[+] and S.Y. Meng[*]
University of Southern California
Los Angeles, California

R. Chow[++]
Grumman Aerospace Corporation
Bethpage, New York

R.C. Smith[**]
NASA Ames Research Center
Moffett Field, California

ABSTRACT

Asymptotic theories for high-aspect-ratio wings in transonic flow developed recently for straight unyawed wings and for oblique wings show that the three-dimensional (3-D) mixed-flow calculations may be reduced to solving a set of 2-D problems at each span station. For wings with surfaces generated from a single airfoil shape, local similitude exists in the 3-D flow structure, permitting the problems to be solved once for all span stations. This paper reviews this theoretical development and the related computational studies. The essential elements in the theory will be identified, their roles are explained; their relationship to the lifting-line theory and related classical methods are discussed. Differences among the pivoted (oblique) wing, the swept-back wing and the swept-forward-wing in the induced upwash are brought out. Examples of similarity solutions are demonstrated for high subcritical and slightly supercritical component flows; comparisons with relaxation solutions to a full potential equation are made. The examples include both oblique and symmetric swept wings, the study also examine the adequacy of the existing full-potential computer code. Outstanding problems remaining for subsequent development are discussed.

1. INTRODUCTION

Our sound understanding in the aerodynamics of wing sweep, and its use to control the compressibility effect, has been limited in the past mostly to problems in the linear flow regimes.[1-5] Recent interest in aircraft wing design has focused on the potentiality for adopting, or modifying, two-dimensional (2-D) supercritical airfoil data for 3-D applications.[6-11] The flow problem in this domain is necessarily nonlinear with a transonic component flow. In this paper, we review theoretical and numerical studies on high-aspect-ratio swept wings for this type of flow, including some very recent works.

Index Categories: Subsonic and Transonic Flow; Aerodynamics; Aircraft Design

[+] Professor, Department of Aerospace Engineering

[++] Senior Staff Scientist, Research Department

[*] Research Assistant, Department of Aerospace Engineering

[**] Senior Research Scientist, Aeronautics Division.

Copyright © American Institute of Aeronautics and Astronautics, Inc., 1980. All rights reserved.

In the domain of interest, the flow field far from the wing section should pertain to a high subsonic, or linear sonic, outer flow, which is representable in the leading approximation by a solution to the Prandtl-Glauert equation corresponding to a swept lifting line (cf. sketches in Fig. 1). Thus, the theoretical treatments[12-18] mentioned must find roots in Prandtl's original lifting-line idea[19], even though the corresponding inner problem to be solved is basically nonlinear and may involve an imbedded supersonic region. Apart from gaining a better physical insight and a greater simplicity in the swept-wing analysis, the approach represented by Refs. 12-18 reflects a desire for implementing the current computer-oriented 3-D methods[20-26] which, though being very powerful, share the common problem of trading accuracy with computer cost and storage requirements, as is well known. While the prospect of the next-generation computers with an equally powerful code development is well in sight[26], they cannot directly answer the question in the aerodynamic theory: namely, in what manner the 2-D component flow on a swept wing is approached, as the wing aspect ratio increases. The least contribution, to which the approach may lead, is providing an asymptotic basis on which the adequacy of the current 3-D codes (their algorithm and some of their implicit assumptions) can be examined.

Detailed expositions of the asymptotic theory underlying this developmentcan be found in Refs. 13-18; the following will address more fully on aspects of interest to the aerodynamic understanding,and on examining its potentiality towards developing less costly computation procedures for aerodynamic design studies.

The following sections will examine the essential elements of the theory, their roles in controlling the induced upwash field and other solution properties. The discussion will bring out a number of aerodynamic features distinguishing oblique (pivoted) wings, the swept-forward wings, conventional swept wings; the delineation will make the distinctions from classical lifting-line analyses apparent. An exposition of the reduced problem of determining the 3-D correction for the (inner) transonic component flow is given in section 3 where some of the subtle differences among Refs. 13-18 will be noted, and the local similarity in the 3-D flow structure as well as an unsteady analogy are explained. The features of a recent development based on the full-potential equations will also be brought out. As in most asymptotic analysis of this type, the theory breaks down locally in a number of regions, of which the most important is perhaps the vicinity of the apex of a swept wing where the

center line has a slope discontinuity; these and other limitations, as well as the fundamental question of perturbing a supercritical shock-free solution are examined in Section 4. Examples of solutions are demonstrated and compared with the full-potential results in Section 5, where some limitation of the existing 3-D full-potential computer codes and a clarification of their formulation are also given.

2. THE ESSENTIAL FEATURES OF THE THEORY

The basic idea used, in common with Prandtl's lifting-line theory[19] for high-aspect-ratio wings, lies in the consideration of two very distinct flow regions: one is a nearly planar (2-D) region next to the wing section with a streamwise length scale comparable to the typical wing chord c_0, and the other is a fully 3-D domain with its size comparable to the wing half-span, b. They are the "inner" and the "outer" region, adopting Van Dyke's[27] terminology. Since the aspect ratio $AR \equiv 2b/c_0$ is high, the flow in the outer region sees the wing and its near wake) as a line of singularity - the lifting line - in the leading approximation.

It may be clearer for the present exposition to begin with the more familiar lifting-line solution for the outer region. It is also convenient to write down here the definitions of the dimensionless inner and outer variables. For the outer region, we will use the variables

$$\bar{x} \equiv x/\sqrt{1-M_\infty^2}\cdot b, \quad \bar{y} \equiv y/b, \quad \bar{z} \equiv z/b, \qquad \bar{\phi} \equiv 2\phi/\alpha_i^{1/2} U_\infty c_0 ; \tag{2.1}$$

and for the inner region, we use the variables

$$\hat{x} \equiv 2x'/c_0, \quad \hat{y} \equiv y'/b, \quad \hat{z} \equiv 2M_\infty \alpha_i^{1/2} z'/c_0, \qquad \hat{\phi} \equiv 2\phi/\alpha_i^{1/2} U_\infty c_0. \tag{2.2}$$

In the above, (x,y,z) is the right-handed Cartesian coordinate system with the x-axis pointing in the free stream direction and z-axis in the lift direction; whereas (x',y',z') is a right-handed orthogonal curvilinear coordinate system with z' = z and y' = 0 being the center line of the wing planform $x = x_c(y)$, and x' is the distance from the center line measured in x-y plane (cf. Fig. 2). It is assumed that the reference center line is located completely in the x-y plane, i.e. we are considering a planar-wing problem. Note that Eqs. (2.1) are in effect the Prandtl-Glauert variables, with the scale for the perturbation potential so chosen to match that of the inner solution; and that Eqs. (2.2) are simply the set suggested by the transonic similarity law for the component flow, using the half reference chord $c_0/2$ as the basic length scale and $U_\infty \equiv U_\infty \cos\Lambda$ as the component free-stream velocity. Here α_i is α/M_∞ with α being taken a typical (absolute) angle of attack, or the wing section thickness. For all practical purposes, we assume γ and α belong to the same order. For convenience in the subsequent discussion on the related classical work, we will employ a dimensionless inner variable $\hat{z}'$ as an alternative to the $\hat{z}$ in Eq. (2.2) namely,

$$\hat{z}' \equiv 2z'/c_0 . \tag{2.3}$$

2.1 The Induced Upwash Field

The perturbation velocity potential $\bar{\phi}_0(\bar{x},\bar{y},\bar{z})$ representing the combined system of the bound and trailing vortices in the outer-flow region, satisfying the Prandtl-Glauert equation, is

$$\bar{\phi}_0 = \frac{\bar{z}}{4\pi}\int_{-1}^{1} \frac{\bar{\Gamma}_0(\bar{y}_1)}{(\bar{y}-\bar{y}_1)^2+\bar{z}^2}\left[1+\frac{\bar{x}-\bar{x}_c(\bar{y}_1)}{\bar{R}_1}\right]d\bar{y}_1 \tag{2.4}$$

$$\bar{R}_1 \equiv \left|\left[\bar{x}-\bar{x}_c(\bar{y}_1)\right]^2+(\bar{y}-\bar{y}_1)^2+\bar{z}^2\right|^{1/2}.$$

The higher approximation of the outer solution

$$\bar{\Phi} = \bar{\phi}_0 + AR^{-1}\bar{\phi}_1 + \cdots \tag{2.5}$$

must account for not only the finite aspect-ratio effect as in Van Dyke's "third-order" theory[27], but also the nonlinearity,[14,18] although the latter will affect little the 3-D corrections to the surface pressure of interest. For the type of center lines considered below, we have either $\bar{x}_c \equiv \beta\bar{y}$ or $\bar{x}_c \equiv \beta|\bar{y}|$, where $\beta \equiv \tan\Lambda/\sqrt{1-M_\infty^2}$.

We point out that the roll-up tendency of the trailing-vortex (TV) sheet far behind the wing is controlled by the trailing vorticity $AR^{-1}d\bar{\Gamma}/d\bar{y}$. Thus, for $AR \gg 1$, the assumption of a flat TV sheet implicit in Eq. (2.3) is seen to be asymptotically correct, as long as $\bar{x} = O(1)$, irrespective of the degree of nonlinearity in the inner flow region (next to the wing section). Therefore, this assumption will not preclude the proper analysis of the large deflection of the TV sheet in the x'-z' plane next to the wing section in a full-potential formulation.[57]

The most crucial knowledge from Eq. (2.4) is the flow behavior in the vicinity of the lifting line, i.e. $\bar{x}-\bar{x}_c(\bar{y}) \to 0$ and $\bar{z} \to 0$, from which the induced velocity, hence the incidence correction, can be determined. For center lines involving only straight segments, the behavior in question can be written as

$$\bar{\phi}_0 \sim \frac{\bar{\Gamma}_0(\bar{y})}{2\pi}\left[\tan^{-1}\left(\frac{\hat{x}}{\sqrt{1-M_\infty^2}}\frac{\hat{z}'}{\hat{z}'}\right)+\frac{\pi}{2}\operatorname{sgn}\hat{z}'\right] + AR^{-1}\frac{\tan\Lambda}{2\pi}\frac{d\bar{\Gamma}_0}{d\bar{y}}\left\{\frac{\hat{z}'}{\sqrt{1-M_\infty^2}}\left[\ln|\hat{\zeta}'| - \ln 2\right] - \hat{z}'\left[\tan^{-1}\left(\frac{\hat{\zeta}}{\sqrt{1-M_\infty^2}}\frac{\hat{z}'}{\hat{z}'}\right)+\frac{\pi}{2}\operatorname{sgn}\hat{z}'\right]\right\} + AR^{-1}\left(\bar{\Sigma}-\bar{\Sigma}_1^c\right)\hat{z}' \tag{2.6a}$$

where $\bar{\Gamma}_0(\bar{y}) \equiv \bar{\Gamma}_0(\bar{y})$, and $\hat{\zeta}' \equiv \hat{x}+i\sqrt{1-M_\infty^2}\,\hat{z}'$. Note that the result has been expressed in the inner variables $\hat{x}$, $\hat{y}$ and $\hat{z}$ to facilitate easy identification for subsequent discussions on the upwash effect; the last term is independent of $\hat{x}$ and $\hat{z}$ with

$$4\pi\bar{\Sigma}(\bar{y}) = -\frac{\sin\bar{\Lambda}}{\sqrt{1-M_\infty^2}}\bar{\Gamma}_0'(\bar{y})\left[2\ln\left(\sqrt{1-M_\infty^2}\,AR\right)+2+\ln\left|(1-\bar{y}^2)\cos^2\bar{\Lambda}\right|\right] + \bar{\Gamma}_0'(\bar{y})\ln\left|\frac{1-\bar{y}}{1+\bar{y}}\cdot\frac{1+\sin\bar{\Lambda}}{1-\sin\bar{\Lambda}}\right| + \int_{-1}^{1}\frac{\bar{\Gamma}_0'(\bar{y}_1)-\bar{\Gamma}_0'(\bar{y})}{\bar{y}_1-\bar{y}}\left[1-\sin\bar{\Lambda}\,\operatorname{sgn}(\bar{y}_1-\bar{y})\right]d\bar{y}_1 , \tag{2.6b}$$

where $\bar{\Sigma}_1^c = 0$ for a straight oblique wing ($\bar{x}_c \equiv \beta\bar{y}$), and

$$4\pi\bar{\Sigma}_1^c(\bar{y}) = \int_{-1}^{1}\frac{\bar{\Gamma}_0(\bar{y}_1)}{(\bar{y}_1-\bar{y})^2}\left[\frac{m(|y_1|-|y|)}{\left|m^2(|y_1|-|y|)^2+(y_1-y)^2\right|^{1/2}} - \sin\bar{\Lambda}\,\operatorname{sgn}(\bar{y}_1-\bar{y})\right]d\bar{y}_1 \tag{2.6c}$$

for a symmetric swept wing ($\bar{x}_c \equiv \beta|\bar{y}|$). In above, $\sin\bar{\Lambda} \equiv \sin\Lambda/\sqrt{1-M_\infty^2}$, and $\cos\bar{\Lambda} \equiv \sqrt{1-M_\infty^2}\cos\Lambda/\sqrt{1-M_\infty^2}$.

Observe that $\bar{\Gamma}_0' = d\bar{\Gamma}_0/d\bar{y} = \sec\Lambda\, d\bar{\Gamma}_0/d\hat{y}$.

The first term on the right of Eq. (2.6a) gives the concentrated vortex representing the wing section, the second group of terms proportional to $A_R'(1-M_\infty^2)^{-1/2}\tan\Lambda\, d\bar{\Gamma}_0/d\hat{y}$, absent in the classical analyses, results from the non-vanishing spanwise component of the near-wake vorticity. This component of the vorticity induces a logarithmically infinite upwash at the center line, as may be anticipated from a consideration of the local irrotational 2-D flow (cf. Fig. 3). This is reflected in the logarithmic dependence of $\bar{\Sigma}$ on the aspect ratio A_R. The terms in Eq. (2.6a) which can be identified with the proper incidence correction (to the inner solution, after properly matching the inner and the outer solution) are

$$\frac{\hat{w}'}{A_R}\left(\bar{\Sigma}+\bar{\Sigma}_0^c - \frac{1}{2\pi}\frac{\sin\Lambda}{\sqrt{1-M_\infty^2}}\frac{d\bar{\Gamma}_0}{d\hat{y}}\ln 2\right) \quad (2.7)$$

[The term with the factor ($\ln 2$) will not be present if the basic length scales for x', etc. is taken to be c_0 instead of $\frac{1}{2}c_0$]. The logarithmic term in $\bar{\Sigma}$ gives a significant contribution of the near wake which is, in turn controlled by the yaw. Similar ($\log A_R$) terms will rise from the center line curvature[14] (or from a time-dependent $\bar{\Gamma}_0$ (37)).

Two observations are essential in subsequent discussions. First, the part of the induced upwash field shown in Eq. (2.6a), which varies with $\hat{x}$ and $\hat{z}$, consists of the concentrated vortex as well as the logarithmic behavior of the near wake; second, since $\log A_R$ results from the logarithmic singularity in the upwash, the $\log A_R$ term would have been absent from the $\bar{\Sigma}$ in Eq. (2.6b) and expression (2.7) above, if the induced incidence correction were taken simply (and incorrectly) as the finite part of the upwash field. In passing, similar results have also been derived for a straight oblique wing by Cook[18], using Mellin transformation techniques.

2.2 Related Classical Analyses

Among the earlier methods applying the lifting-line idea to swept wings (see Ref. 3, 28-30 for a thorough review), the most well known is perhaps that of Weisinger[28]. As pointed out by Jones and Cohen[3], Weisinger's method does not recover correctly the limit for the infinite aspect ratio. We may recall that in Weisinger's method, the bound vortices at each wing section are represented by a concentrated vortex at the 1/4 chord point and the induced downwash (negative upwash) is computed at the 3/4 chord point. Nevertheless, the logarithmic dependence on A_R, mentioned should be found also in solutions by the Weisinger method (applied to high-aspect-ratio wings), since an upwash formula equivalent to Eq. (2.4) was used therein. On the other hand, the use of the 3/4 chord as an upwash control point requires a uniform upwash, or one varying linearly in x'; but this requirement is not met by Eq. (2.6a). In addition, its validity also imply the assumption of a local 2-D component flow devoid of the near wake, which is again contrary to Eq. (2.6a). Its failure in the high-aspect-ratio range, therefore, should not be too surprising.

This comment does not apply directly to the vortex-lattice method[31,32] employing the 3/4 chord as a control point for each lattice (panel). This is because the large upwash and spanwise-vorticity jump associated with the logarithmic singularity depend mainly on the vortex-shedding rate of the individual lattice, whose contribution is made smaller as the lattice number increases. [Error of such a nature will nevertheless remain.]

Solutions to elliptic lifting surface at yaw have been given early by Krienes in Ref. 33, where solutions to the inverse lifting problem were superimposed to determine lift and moments of a 5:1 elliptic flat plate at yaw (a helpful delineation of Krienes' analysis in the unyawed case can be found in Ref. 3). Of the five-term truncated series used therein, three terms were symmetric spanwise, it is not clear if the remaining terms could adequately describe the asymmetric span load of interest. Generalization of the lifting-line theory for a wing with a curved center line, as well as a wing in side slip, has been considered by Dorodnitsyn[34] who noted the significance of the logarithmically large upwash effect due to yaw.* However, the analysis involved the 3/4 chord controlled point, as in Weisinger's[28], and therefore the 3-D effect analyzed cannot be expected to be asymptotically correct. The results were, in any case, restricted to small departure from a straight, unswept center line in the linear regime.

A case of curved center line has been studied by Thurber[35] who considered a crescent-moon-shaped wing from the viewpoint of an asymptotic theory; however, the solutions for the region around the wing section and the matching problem were not considered (the upwash calculation also contained errors). Oscillating high-aspect-ratio wings with curved center lines have been treated by the senior author in Ref. 36, where the basic reasons for the appearance of a logarithmically large upwash are explained.

2.3 The Asymptotic Approach and the Basic Features of the Theory

The works under review adopt the basic approach initiated by Van Dyke[27] who considered Prandtl's lifting-line theory as the leading approximation in an asymptotic analysis for a high-aspect-ratio wing. While this more formal approach may break down near the tip of a rectangular or taper wing (where the asymptotic expansion is non-uniform, as is quite well known), the methods allow a systematic improvement by successive approximations, and a clearer delineation of the various competing 3-D effects. Thus Van Dyke is able to extend Prandtl's work for a straight, unswept wing to a higher order[38]. On account of the tip nonuniformity, however, the third-order results of Ref. 37 does not predict correctly the total lift and drag; there is, in addition, an error related to the Kutta condition, to be discussed later.

An example of the asymptotic analysis of this type, representing a significant departure from the assumption of a straight, unswept center line, is given in Refs. 12 (a) and (b) for an oblique wing in the framework of the linear theory of an incompressible flow. This linear analysis shares the same outer solution and the corresponding upwash distribution in the subsequent transonic oblique-wing analyses[13,14]. The rather encouraging

*This work was called to our attention by Drs. G. Daforno and R.E. Melnik of the Grumman Aerospace Corporation.

comparison with the more exact wing-panel method given therein suggests that equal success may be obtained for the transonic swept-wing analyses[13-18] at least for the oblique wings+.

(i) Departure from the classical analysis

Aside from the interesting dependence of the induced upwash on the span loading $\bar{\Gamma}_o(\bar{y})$ and on the sweep angle Λ, to be delineated more fully later, there are other features in the formulation, which represent important departures from the classical theory. One of these is the need for considering the spanwise component of the trailing vorticity between the trailing edge and the downstream infinity in the reduced inner problem. Such a need is made evident by the flow behavior shown in Eq. (2.6a) where the second term gives a jump in $\partial\Phi_o/\partial\hat{z}$ across the wing trace, being proportional to $-\tan\Lambda\,\tilde{R}_1^{-1}\,d\bar{\Gamma}_o/d\bar{y}$. This means that the local component flow cannot be determined by a simple incidence correction to a wakeless 2-D component flow as in Prandtl's original analysis. The solution presented for the straight oblique wing in Refs. 12 (a) and (b) confirms the importance for treating the vorticity jump at the wing trace. In the more general cases[14,36] the partial differential equation (PDE) governing the inner region must also be corrected for the center-line curvature and/or for a 3-D compressibility effects (see below).

One must observe that, as the component Mach number M_n approaches one (from below), the sweep angle Λ must necessarily decrease toward zero (unless $M_\infty > 1$). According to Eq. (2.6a), a smaller Λ will not diminish the importance of the logarithmic upwash field associated with the spanwise near-wake vorticity, but reduce at the same time the spanwise component of the wake-vorticity itself. For this reason, the velocity will remain essentially continuous across the wing trace in the inner problem for transonic swept wings.

(ii) Kutta condition

The Kutta condition at the trailing edge plays an important role in the present theory. While an infinite (integrable) singularity in the 3-D correction to the surface speed could suggest only a local breakdown (nonuniform) of the asymptotic solution near the trailing edge, it gives an erroneous correction for the entire wing section. This is because the latter represents an unwanted eigen solution to the homogeneous boundary-value problem, as is shown quite clearly by the explicit inner solution in Refs. 12 for an oblique-wing. Similar problems appear for the unyawed straight wing at the "third order" where the particular solution to the inner problem given originally in Refs. 27 and 37 violates the Kutta condition, as being uncovered and corrected by Kida and Miyai[38].

2.4 Behavior of the Induced Upwash on Swept Wings

The part of induced upwash distribution in the form of $\bar{\Sigma}_o$ is dominated by the term $-(2\pi)^{-1}(1-M_n^2)^{-1/2}\cdot\sin\Lambda\, d\bar{\Gamma}_o/d\bar{y}\,\ln(\sqrt{1-M_n^2}\,\tilde{R}_1)$ which will generally reduce the downwash on an aft (or swept-back wing) panel where $d\bar{\Gamma}_o/d\bar{y} < 0$ and augment the downwash on the forward panel where $d\bar{\Gamma}_o/d\bar{y} > 0$. For most span loadings of interest, $d\bar{\Gamma}_o/d\bar{y}$ tends to infinity at the tip $\bar{y} = \pm 1$ like $(1-\bar{y}^2)^{-1/2}$; this, together with the logarithm involving $\tilde{R}_1 \equiv \sqrt{1-M_n^2}\,R_1$ and $(1-\bar{y}^2)$ leads to a maximum of $O(\tilde{R}_1^{-1/2})$ near the tip of a swept-back panel.

There is also a minimum in $\bar{\Sigma}$ near the tip on an swept-forward panel (where the downwash reaches a magnitude of $O(\tilde{R}_1^{-1/2})$). Although the magnitude of the induced velocity becomes infinite at the tip, $\bar{\Sigma}$ reverses its sign and vanishes at a span station extremely close to the tips. This tends to provide a reasonable description of the span loading, in spite of the local breakdown at the tip. The latter's region of nonuniformity is estimated to be $\bar{y} \pm 1 = O(\tilde{R}_1^{-2}\ln\tilde{R}_1)$.

The asymmetrical span loading contributed by terms proportional to $-d\bar{\Gamma}_o/d\bar{y}$ in $\bar{\Sigma}$ are responsible for the unbalanced rolling moment of an oblique (pivoted) wing, unless twist, wing bend, or special pivot location is introduced in the design[5,11]. The extent to which this asymmetry depends on the yaw angle $\bar{\Lambda}$ and on the type of the basic span loading $\bar{\Gamma}_o(\bar{y})$ is illustrated in Fig. 4 where the upwash functions $\bar{\Sigma}(\bar{y})$ for oblique wings with an elliptic and with an extended-span (ES) distribution in $\bar{\Gamma}_o(\bar{y})$ are shown for $\bar{\Lambda} = 0$, 22.5° and 45°. These $\bar{\Sigma}$'s were computed from Eq. (2.6) with $\bar{\Sigma}(\bar{y})$ normalized by the mid-span value of $\bar{\Gamma}_o$, and the (reduced) aspect ratio taken to be such that $\tilde{R}_1 \sec\Lambda = 8.4$. We note that the graphs can be corrected for other aspect ratio by simply adding to

$$\Delta\bar{\Sigma} = -\frac{1}{2\pi}\cdot\frac{\sin\bar{\Lambda}}{\sqrt{1-M_n^2}}\cdot\bar{\Gamma}_o'(\bar{y})\cdot\ln\left|\frac{\tilde{R}_1\sec\Lambda}{8.4}\right| \qquad (2.8)$$

The ES load considered has a root-bending moment equal to that of an elliptic load for the same lift but lesser drag[40]. The span however is longer, hence the name "extended span". For the ES distribution shown, the extended span is 1.15 times that of the elliptic one.

We note in passing that at $\bar{\Lambda} = 0$, the ES load induces a lineal distribution in the upwash, equivalent to the effect of a wash-in, and the asymmetry caused by the yaw will further increase this effect on the downstream side, turning a regular downwash into a (positive) upwash on the aft-panel tip. The amplification of the induced velocity in the out board region of each panel, and the existence of a maximum and a minimum in the manner discussed earlier, are quite apparent from the figure.

The induced flow-angle correction will depend also on the center-line geometry. Fig. 5 shows the span distribution of normalized $\bar{\Sigma} + \bar{\Sigma}_o^c$ for symmetric swept-foward and swept-back wings, at different degrees of sweep. It is assumed in the calculations that the span loading $\bar{\Gamma}_o(\bar{y})$ (based on the strip theory) is elliptic, and the (reduced) aspect ratio $\tilde{R}_1 \equiv \sqrt{1-M_n^2}\,R_1$ is 9.26. Results for five values of $\bar{\Lambda}$ (0, ±22.5°, ±45°) are shown. At $M_\infty = 0.755$, $\bar{\Lambda} = \pm 22.5°$ and $\pm 45°$ corresponds to $\Lambda = \pm 15.2°$ and $\pm 33.33°$, respectively.

The familiar fact about the need for a washout on a swept-back wing is quite evident from the large reduction in $|\bar{\Sigma} + \bar{\Sigma}_o^c|$ near the tip shown.

+ The scales in the span loadings shown in Fig. 3 of Ref. 12(a) and in Figs. 4-6 of Ref. 12(b) are incorrect; they should all be reduced by a factor of 10.

The usefulness of adopting a forward sweep ($\bar{\Lambda} < 0$) in counteracting the above effect is also quite evident from Fig. 5.

For value of $\bar{\mathcal{R}}_1$ other than 9.26, the correction to $\bar{\Sigma}$ indicated in Eq. (2.19) again applies. The behavior near the tip of a swept wing is again similar to that observed earlier for the oblique wing; but in approach the center corresponding to the wing appex, the magnitude of the induced upwash becomes unbounded. This divergence is expected from $\bar{\Sigma}_0^c$ which, upon $\bar{y} \to 0$, yields

$$\bar{\Sigma}_0^c \sim -\bar{f}_0'(0)\,\frac{\sin\bar{\Lambda}}{4\pi\bar{y}} \qquad (2.9)$$

This is well borne out in the 45° swept-back case, for which the downwash near the center is more severe than other cases shown. Unless $\bar{f}_0'(0) = 0$, the theory will break down at $\bar{y} = 0$. Comparing $(\bar{\Sigma} + \bar{\Sigma}_0^c)\bar{\mathcal{R}}_1^{-1}$ with the leading term in Eq. (2.6a), in conjunction with Eq. (2.9), reveals readily that a complete break down occurs where $(1-M_n^2)^{-1/2} \cdot \bar{\mathcal{R}}_1^{-1}\sin\bar{\Lambda}\,\bar{f}_0'(\bar{y})/\bar{y}$ becomes of unit order, i.e. at

$$\bar{y} = O\left[\frac{\sin\bar{\Lambda}\,\bar{f}_0'(0)}{(1-M_n^2)\,\bar{\mathcal{R}}_1}\right] \qquad (2.10)$$

This nonuniformity will be discussed further later in the context of the nonlinear transonic flow. In passing, we note that unlike the upwash on a swept-back wing, the $\bar{\Sigma} + \bar{\Sigma}_0^c$ near the apex station of a swept-forward wing does not become excessively large until $\bar{y}$ comes very close to the origin. Thus, break down of the theory near $\bar{y} = 0$ may be less severe for the swept-forward case.

3. TRANSONIC SWEPT WING: THE INNER PROBLEM

We consider high subsonic flight near the speed of sound. As is well known, the performance of a transonic wing is limited by the rapid drag rise as $M_\infty \to 1$. With a moderate sweep, however, one can bring the flight Mach number of a high aspect ratio wing closer to one, while keeping the component flow around the wing section at the verge of the drag rise.

3.1 Basic Parameters and PDE

The basic component flow in this situation is necessarily nonlinear and of a mixed (hyperbolic-elliptic) type; if the wing section is sufficiently thin, this component flow at each span station will obviously be controlled by the transonic similarity parameter based on the component Mach number $M_n = M_\infty \cos\Lambda$

$$K_n \equiv \frac{1-M_n^2}{\alpha^{2/3} M_n}, \qquad (3.1a)$$

familiar from the transonic small-disturbance theory[40-43]. On account of the stronger spatial attenuation for disturbances in a 3-D flow field, it is possible to match this predominately 2-D nonlinear inner flow with a basically linear outer flow described earlier. As observed in § 2, the swept angle Λ must be confined to a relatively narrow range, because, if Λ is too small, M_n will exceed the drag-rise value of the wing section, and if Λ is too large, the M would become so far from unity that the advantage of a high pressure coefficient will be lost. The Λ range of interest is that which will keep K_n at the unit order, while M_∞ does not exceed one. Let

$$\textcircled{M} \equiv \frac{\Lambda}{\alpha^{1/3}}. \qquad (3.1b)$$

The foregoing condition is then equivalent to the requirement $\textcircled{M} = O(1)$. Finally, there is a reduced aspect ratio controlling the 3-D influence, the reciprocal of which is

$$\epsilon \equiv \frac{1}{\alpha^{1/3}\mathcal{R}_1}. \qquad (3.1c)$$

Note that $\alpha^{1/3}\mathcal{R}_1 = (M_n K_n)^{-1/2}\bar{\mathcal{R}}_1$. The asymptotic analyses of Refs. 13-18, including the unswept case, pertain to the limit $\epsilon \to 0$, while keeping K_n and $\textcircled{M}$ (also $\alpha^{1/3}\epsilon^{-1}$) fixed. With the additional requirement $M_\infty < 1$, the conditions on $\textcircled{M}$ and K_n amount to

$$\textcircled{M}^2 < K_n = O(1) \qquad (3.2)$$

When the center-line curvature is taken to be zero locally, and the disturbance is assumed to be sufficiently weak, the PDE in the flow region next to the wing under conditions just mentioned can be obtained from an expanded form of the full potential equation in the rotated coordinates (x', y', z') as

$$(1-M_n^2)\,\phi_{x'x'} + \phi_{y'y'} + \phi_{z'z'} - 2M_n^2\tan\Lambda\,\phi_{x'y'} - M_n^2 U_n^{-1}\left(1+\tfrac{\gamma-1}{2}M_n^2\right)\frac{\partial}{\partial x'}\phi_{x'}^2 + \cdots = 0, \qquad (3.3)$$

where the terms omitted $(\cdots)$ can be shown to be relatively small on the basis of the transonic small-disturbance assumption [i.e. $1-M_n^2 = O(\alpha^{2/3})$, $\phi = O(U_n c_n \alpha^{2/3})$, $\partial/\partial x' : \partial/\partial z' = 1 : O(\alpha^{1/3})$]. Except for the third term, the equations shown above are familiar from the transonic small-disturbance (TSD) theory[40-44]. The added term, $-2M_n^2\tan\Lambda\,\phi_{x'y'}$ results from a 3-D compressibility correction to the velocity divergence (owing to the spanwise variation of the density) and will remain also in the linear regime, unless M_n or $\tan\Lambda$ vanishes. In terms of the inner variables [cf. Eq. (2.2)] the above equation can be written as

$$\frac{\partial}{\partial\hat{x}}\left[K_n\hat{\phi}_{\hat{x}} - \tfrac{\gamma+1}{2}\hat{\phi}_{\hat{x}}^2\right] + \hat{\phi}_{\hat{z}\hat{z}} = 2\textcircled{M}\epsilon\,\hat{\phi}_{\hat{x}\hat{y}} + \cdots \qquad (3.4)$$

with the remainder being comparable to ϵ^2. Thus the 3-D compressibility correction appears as a correction to the Von Kármán equation[40] and the reason for introducing the reduced sweep angle $\textcircled{M} \equiv \Lambda/\alpha^{1/3}$ is made apparent. A pressure coefficient may be computed from the solution as

$$C_p \equiv \frac{p-p_\infty}{\frac{1}{2}\rho_\infty U_\infty^2} = -2\cos^2\Lambda\,\alpha^{2/3}\hat{\phi}_{\hat{x}} + \cdots \qquad (3.5)$$

With a remainder comparable to ϵ^4. Note that as long as $\textcircled{M} = O(1)$, i.e. $\Lambda = O(\alpha^{1/3})$, C_p is unaffected by $\hat{\phi}_{\hat{y}}$.

We note that in the transonic similarity parameter defined in Eq. (3.1a), the denominator is taken as the first power of M_n as in Murman and Cole[43] also Murman and Krupp[45]. This choice gives a definite improvement in the accuracy of the critical flow speed, hence, the wave pattern near the sonic boundary, as pointed out in Ref. 14(b) and in Ref. 46. One also may note that most of the

"$\cos\Lambda$" factors appearing in Eqs. (2.2), (3.4) - (3.7), except that in $(1-M_\infty^2)$ of K_n, can be replaced by unity because of $\Theta = O(1)$. However, its retention in Eqs. (2.2) and (3.5) will allow a greater range of the sweep angle Λ for the validity of the theory[14b].

3.2 Conditions on Wing Surface, Wing Trace and Shock

For an impermeable thin wing surface with the leading and trailing edges in the wing plane described by $\hat{x} = \hat{a}(\hat{y})$ and $\hat{x} = \hat{b}(y)$, respectively, the ordinate can be written as

$$z' = \frac{c_r}{2}\left[\alpha\,\hat{Z}^{\pm}(\hat{x},\hat{y}) + \alpha^{1/3}\hat{Z}_B(\hat{y}) + \right.$$
$$\left. + \alpha\epsilon(\hat{x}-\hat{x}_0)\,\hat{I}(\hat{y})\right], \qquad (3.6)$$

where $\hat{Z}^{\pm}$, $\hat{Z}_B$, and $\hat{I}$ are all of unit order, and the "$\pm$" in $\hat{Z}^{\pm}$ signifies the two different distributions for the upper and the lower surfaces. The functions $\hat{Z}_B(\hat{y})$ and $\hat{I}(\hat{y})$ represent, respectively, a wing twist and an (upward) wing-bend; they are introduced to allow control of the 3-D effect. The wing boundary condition can be transferred to the wing plane ($\hat{z} = 0$) to read

$$\left(\frac{\partial\hat{\phi}}{\partial\hat{z}}\right)_w = \frac{\partial}{\partial\hat{x}}\hat{Z}^{\pm} + \epsilon\Theta\frac{d}{d\hat{y}}\hat{Z}_B + \epsilon\hat{I}\,, \qquad (3.7)$$

where the subscript "w" refers to the wing. On the wing trace at $\hat{z} = 0$ corresponding to the vortex sheet, the small-disturbance approximation gives the requirements that pressure jump and the normal velocity are zero. In view of Eq. (3.5), this leads to the condition that the two components of the velocity perturbation, $\hat{\phi}_{\hat{x}}$ and $\hat{\phi}_{\hat{z}}$ are required to be continuous across the wing trace. Therefore, in solving for the 3-D correction for the inner solution, we can treat the problem as being wakeless. This simplicity follows from the fact already noted that the spanwise component of the wake-vorticity is not large enough to warrant consideration in as much as Λ is small.

The PDE (3.4) is of a mixed type depending on K_n and $\hat{\phi}_{\hat{x}}$; the characteristic surface of the hyperbolic region, $\hat{x} = \hat{x}^c(\hat{z},\hat{y})$ is given by[47]

$$K_n - (\gamma+1)\hat{\phi}_{\hat{x}} + 2\epsilon\Theta\frac{\partial\hat{x}^c}{\partial\hat{y}} = -\left(\frac{\partial\hat{x}^c}{\partial\hat{z}}\right)^2. \qquad (3.8)$$

In the limit $\epsilon \to 0$, we identify the critical speed for the 2-D component flow

$$\hat{\phi}_{\hat{x}} = \hat{u}_* \equiv \frac{K_n}{\gamma+1}\,. \qquad (3.9)$$

The PDE (3.4) admits weak solutions with discontinuity surface consistent with the Rankine-Hugoniot shock relations under the TSD approximation. One of the jump condition is of the same form as the characteristic equation (3.8), with $\hat{x}^c(\hat{y})$ there replaced by $\hat{x}^D(\hat{y})$ (the superscript "D" refers to the shock discontinuity) and $\hat{\phi}_{\hat{x}}$ replaced by the arithmetical mean of $\hat{\phi}_{\hat{x}}$ across the shock. The other condition governing the shock, corresponding to the continuity of the tangential velocity, can be simply taken to be the continuity of $\hat{\phi}$.

3.3 Perturbation Analysis

As seen above, the 3-D correction considered represents a small peturbation of the basic 2-D component flow. The analysis can be made more systematic by solving for the coefficients in the asymptotic expansion for small ϵ:

$$\hat{\phi} = \hat{\phi}_0 + \epsilon\hat{\phi}_1 + \cdots \qquad (3.10a)$$

with a corresponding expansion for the unknown shock boundary

$$\hat{x} = \hat{x}_0^D(\hat{z};\hat{y}) + \epsilon\hat{x}_1^D(\hat{z};\hat{y}) + \cdots \qquad (3.10b)$$

where a weak logarithmic dependence of $\hat{\phi}_1$ and $\hat{x}_1^D$ on ϵ is expected (in view of the nature of the upwash examined in §2). The resulting equation of particular interest is PDE governing

$$\left\{\left[K_n-(\gamma+1)\hat{\phi}_{0\hat{x}}\right]\frac{\partial^2}{\partial\hat{x}^2} + \frac{\partial^2}{\partial\hat{z}^2} - (\gamma+1)\hat{\phi}_{0\hat{x}\hat{x}}\frac{\partial}{\partial\hat{x}}\right\}\hat{\phi}_1$$
$$= 2\Theta\,\hat{\phi}_{0\hat{x}\hat{y}} \qquad (3.11)$$

The nonhomogeneous term on the right results from the 3-D compressibility correction, it confirms the remark given earlier (§2) that the upwash correction alone does not give the complete answer to the 3-D potential problem.

As in most standard perturbation analysis involving shock waves, the jump conditions are analytically transferred from $\hat{x} = \hat{x}^D(\hat{z};\hat{y})$ to the unperturbed boundary $\hat{x} = \hat{x}_0^D(\hat{z};\hat{y})$ where the resulting condition for $\hat{\phi}_1$ and $\hat{x}_1^D$ read

$$2\Theta\frac{\partial\hat{x}_0^D}{\partial\hat{y}} - (\gamma+1)\left\langle\hat{\phi}_{1\hat{x}} + \hat{x}_1^D\hat{\phi}_{0\hat{x}\hat{x}}\right\rangle$$
$$= -2\frac{\partial\hat{x}_0^D}{\partial\hat{z}}\cdot\frac{\partial\hat{x}_1^D}{\partial\hat{z}}\,, \qquad (3.12a)$$

$$\left[\!\left[\hat{\phi}_1 + \hat{x}^D\hat{\phi}_{0\hat{x}}\right]\!\right] = 0 \qquad (3.12b)$$

where $\langle\ \rangle$ and $[\![\ ]\!]$ stands for the arithmetical mean and the difference across the discontinuity surface, respectively.

3.4 The Far Field of the Inner Solution

At a point sufficiently far from the wing section, the solutions $\hat{\phi}_0$ and $\hat{\phi}_1$ admits a behavior, apparent from the governing PDE,

$$\hat{\phi}_0 \sim \frac{\hat{\Gamma}_0}{2\pi}\left[\tan^{-1}\left(\frac{\hat{x}}{\sqrt{K_n}\,\hat{z}}\right) + \frac{\pi}{2}\,\mathrm{Sgn}\,\hat{z}\right] + \cdots \qquad (3.13a)$$

$$\hat{\phi}_1 \sim \frac{\Theta\,\hat{z}}{2\pi\sqrt{K_n}}\cdot\frac{d\hat{\Gamma}_0}{d\hat{y}}\cdot\ln|\hat{\zeta}| - \hat{C}_1^{\ell}\sqrt{K_n}\,\hat{z} + \hat{C}_1^{r}\hat{x} + \cdots$$

where

$$\hat{\zeta} \equiv \hat{x} + i\sqrt{K_n}\,\hat{z}\,. \qquad (3.13b)$$

As well known, the behavior shown in (3.13a) represents a concentrated vortex with a circulation equal to the potential jump at the trailing edge. The leading term in Eq. (3.13b) is simply the contribution of $-z\Theta\hat{\phi}_{0\hat{x}\hat{y}}$ on the RHS Eq. (3.11), using Eq. (3.13a). The next two terms in Eq. (3.13b) are simply the two components of the induced velocity to be determined by matching with the outer solution.

The remainder of (...) in (3.13a) is comparable in magnitude to the doublet, i.e. to $|\hat{\zeta}|^{-1}$, including terms proportional to $\hat{\Gamma}'\hat{x}\ln|\hat{\zeta}|/|\hat{\zeta}|^2$ and $\hat{\Gamma}'\hat{x}^2/|\hat{\zeta}|^4$, as is quite well known from the 2-D TSD analyses. The remainder (...) for $\hat{\phi}_1$ in (3.13b) is comparable to unity, (to be more precise, to $(\ln|\hat{\zeta}|)^2$, $\ln|\hat{\zeta}|$ and unity), including terms

proportional to $\hat{\Pi}_o^2$ as well as the doublet strength in the far-field of $\hat{\phi}_0$. It must be pointed out that these remainders are not essential for formulating the reduced problems for $\hat{\phi}_0$ and $\hat{\phi}_1$, but its use at the far boundary in a numerical computation proves to be very helpful[13,14].

3.5 A Line-Source Effect

Among the logarithmic terms mentioned is a (pure) line-source term $\hat{Q}_1(2\pi)^{-1}\ln|\hat{\zeta}|$. Its existance could have been anticipated from the appearance of the source-like 3-D compressibility correction on the RHS of PDE (3.4) or (3.11). Ref. 14(a) shows that, for a straight center line, the source strength $\hat{Q}_1(\hat{y})$ can be explicitly computed from one of the doublet strength belonging to the far-field expression of $\hat{\phi}_0$; the result is also applicable in cases involving piecewise straight segments.† This and another term of the order $|\log|\hat{\zeta}|$ are not found however in Cook's analysis[18].

The existence of a nonvanishing Q_1 can be readily demonstrated for cases in which $\hat{\Pi}_o^2$ can be neglected. Note Eq. (3.11) becomes

$$\left(\frac{\partial^2}{\partial\hat{x}^2}+\frac{\partial^2}{\partial\hat{y}^2}\right)\hat{\phi}_1 \sim 2\frac{M}{K_n}\frac{\partial^2}{\partial\hat{x}\,\partial\hat{y}}\hat{\phi}_o \qquad (3.14)$$

in the far-field ($|\hat{\zeta}|\to\infty$). In this case, the area integral of the RHS of Eq. (3.14) can be equated to the total volume flux; therefore,

$$\hat{Q}_1 = \frac{2M}{K_n}\iint\frac{\partial^2}{\partial\hat{x}\partial\hat{y}}\hat{\phi}_o\,d\hat{x}\,d\hat{y}$$

$$=\frac{2M}{K_n}\lim_{|\hat{\zeta}|\to\infty}\oint\frac{\partial}{\partial\hat{y}}\hat{\phi}_o\,d\hat{y} = \frac{2M}{K_n}\pi\frac{d\hat{D}_o^r}{d\hat{y}}\,, \qquad (3.15)$$

where $\hat{D}_o^r$ is the far-field doublet strength of $\hat{\phi}_0$ associated with the airfoil thickness. It is thus seen that the swept or oblique wing will present a line-source effect in the outer flow, which must be taken into account in a third-order theory (in Van Dyke's sense[27, 37]), even in the linear case. This line-source will not affect the lifting part of the linear problem, of course.

3.6 Matching with Outer Solution

In the inner variables $\hat{x},\hat{y}$ and $\hat{z}$, the behavior of the outer solution near the centerline, Eq. (2.6a), can be expressed as[14b]

$$\bar{\phi}_o \sim \frac{\bar{\Pi}((\hat{y}))}{2\pi}\left[\tan^{-1}\left(\hat{x}/\sqrt{K_n}\,\hat{z}\right)+\frac{\pi}{2}\,Sgn\,\hat{z}\right]+$$
$$+\epsilon\frac{M}{\sqrt{K_n}}\frac{1}{2\pi}\frac{d\bar{\Pi}_o}{d\hat{y}}\hat{z}\left[\ln|\hat{\zeta}|-\ln 2\right]-$$
$$-\alpha^{2/3}\epsilon M\frac{1}{2\pi}\frac{d\bar{\Pi}_o}{d\hat{y}}\left[\tan^{-1}\left(\hat{x}/\sqrt{K_n}\,\hat{z}\right)+\frac{\pi}{2}\,Sgn\,\hat{z}\right]+$$
$$+\epsilon\left(\bar{\Sigma}+\bar{\Sigma}_o^c\right)\hat{z}+\cdots \qquad (3.16)$$

where we have omitted all factors of M_n, such as $M_n^{2/3}$ in $\tan^{-1}(M_n^{3/2}\hat{x}/\sqrt{K_n}\,\hat{z})$, since its error can affect the determination of $\bar{\Pi}_o((\hat{y}))$ at most to the order $\alpha^{2/3}$ or ϵ^2, which in turn can influence the inner solution through the upwash correction to the order ϵ^3, at the most. The third term on the RHS of Eq. (3.16) confirm the anticipation that the spanwise vorticity jump can be neglected, which is seen to be proportional to $\alpha^{2/3}\epsilon$, hence comparable to ϵ^3.

Comparing Eq. (3.16) with the corresponding far-field behavior of the inner solution $(\hat{\phi}_0+\epsilon\hat{\phi}_1+\cdots)$, and noting the slight difference in the definitions of $\bar{\phi}$ and $\hat{\phi}$, we can now identify $\bar{\Pi}_o(y) \equiv \bar{\Pi}_o((y))$ with $\cos^{1/3}\Lambda\,\hat{\Pi}_o(\hat{y}) \approx \bar{\Pi}_o(\hat{y})$, and the induced velocity correction with $(\bar{\Sigma}+\bar{\Sigma}_o^c)$:

$$\hat{C}_1^r(\hat{y}) = 0\,,$$
$$-\sqrt{K_n}\,\hat{C}_1^i(\hat{y}) = \bar{\Sigma}-\bar{\Sigma}_1^c - \frac{\ln 2}{2\pi}\frac{M}{\sqrt{K_n}}\frac{d\bar{\Pi}_o}{d\hat{y}} \qquad (3.17)$$

With these identifications, the inner and outer solution shown in Eqs. (3.13) and (3.16) are seen to match [for all terms shown, except the third (higher-order) term in Eq. (3.16)]. Ref. 14 also confirms the matching to a higher order in $|\hat{\zeta}|^{-1}$ and ϵ between $(\bar{\phi}_0+\epsilon\bar{\phi}_1)$, and $(\hat{\phi}_0+\epsilon\hat{\phi}_1)$, in which the strengths of the line doublet, the vortex, and the line-source for the outer $\bar{\phi}_1$ solution are determined.

With $\hat{C}_1^r$ and $\hat{C}_1^i$ now determined in terms of $\hat{\Pi}_o(\hat{y})$, it is assumed that the inner solutions for $\hat{\phi}_0$ and $\hat{\phi}_1$, which fulfill the Kutta condition and are continuous everywhere except across the wing and in the wing trace ($\hat{x}>\hat{a}$, $\hat{z}=\pm 0$), are uniquely determined by their PDE's, together with their respective conditions on the wing and on the wing trace and the far-field conditions Eq.(3.13).

The problem of swept wing is thus reduced to solving first a strictly 2-D system involving the nonlinear TSD Eq. (3.4) for $\hat{\phi}_0$ with its right-hand member omitted, and $\hat{\Phi}$ therein replaced by $\hat{\phi}_0$, and next, solving another 2-D (linear) PDE system with the PDE (3.11) for the 3-D correction $\hat{\phi}_1$. The spanwise variable $\hat{y}$ appears in the two (uncoupled) PDE system only as a parameter through the wing and the far boundary conditions. The solutions at each span station can be determined independently of another, except for the spanwise distribution of $\hat{\Pi}_o(\hat{y})$ and $\hat{\phi}_0\,\hat{x}\,\hat{y}$, which can be obtained after $\hat{\phi}_0$ has been determined from an adequate number of span stations.

3.7 Superposition of Similarity Solutions For $\hat{\phi}_1$

Owing to the linearity, the 3-D correction to $\hat{\phi}_1$ can be decomposed into separate parts. There is an important class of wing surface geometry, for which each of these separate parts (after being suitably scaled), has similarity solutions independent of $\hat{y}$, as does the basic solution $\hat{\phi}_0$. Thus, the reduced 2-D equation system in this case can be solved once for all span stations. [This interesting solution stucture does not appear to be recognized by Cook in her analysis[18].]

This wing class requires that the wing section at each span station be generated from a single airfoil profile, but the local chord c(y) may vary; local twist and/or wing bend for compensating the 3-D effect are also allowed, as in Eq. (3.6). This geometry can be more specifically written as

$$z' = \frac{c}{2}\left[\alpha\hat{c}(\hat{y})\,\hat{Z}^{\pm}\left(\frac{\hat{x}}{\hat{c}}\right)+\alpha^{1/3}\hat{Z}_0(\hat{y})+\alpha\epsilon(\hat{x}-\hat{x}_0)\hat{I}(\hat{y})\right] \qquad (3.18)$$

where $\hat{c}(\hat{y}) \equiv c(y)/c_0$. Implicit in Eq. (3.18) is that the center-line $\hat{x}=\hat{z}=0$ is the common straight axis for the similar wing sections at different span stations; the percentage-chord location of this straight axis can be arbitrarily chosen, however.

To describe the flow structure in question, we shall rescale $\hat{\phi}$, $\hat{x}$ and $\hat{z}$ by the local chord c(y), and introduce the variables

$$\tilde{x}=\hat{x}/\hat{c}\,,\quad \tilde{z}=\hat{z}/\hat{c}\,,\quad \tilde{y}=\cos\Lambda\,\hat{y}\,,\quad \tilde{\phi}=\hat{\phi}/\hat{c} \qquad (3.19)$$

The similarity flow structure admissible under Eq.

† $\hat{Q}_1$ also depends on $\hat{\Pi}_o^2$.

(3.18), with due allowance for the upwash corrections, is represented by

$$\tilde{\Phi} = \tilde{\Phi}_0(\tilde{x},\tilde{z}) + \epsilon\Theta\hat{C}'\tilde{\Phi}_1(\tilde{x},\tilde{z}) - \epsilon\sqrt{K_n}\tilde{C}_1^i\tilde{z} + \\ + \epsilon\left[\sqrt{K_n}\hat{C}_1^i(\tilde{y}) + \hat{I}(\tilde{y}) + \Theta\hat{Z}_0'(\tilde{y})\right]\tilde{\Phi}_2(\tilde{x},\tilde{z}) \qquad (3.20a)$$

where $\hat{C}' \equiv d\hat{C}/d\tilde{y}$, and $\tilde{\Phi}_0$, $\tilde{\Phi}_1$, and $\tilde{\Phi}_2$ are independent of $\tilde{y}$. The corresponding shock geometry, when an imbedded supercritical flow region appears, takes on a similar form

$$\tilde{x} = \tilde{x}_0^D(\tilde{z}) + \epsilon\Theta\hat{C}'\tilde{x}_1^D(\tilde{z}) + \\ + \epsilon\left[K_n\tilde{C}_1^i(\tilde{y}) + \hat{I}(\tilde{y}) + \Theta\hat{Z}_0'(\tilde{y})\right]\tilde{x}_2^D(\tilde{z}) \qquad (3.20b)$$

The third term of Eq. (3.20a) is introduced so that the upwash effect is transferred through the solution $\tilde{\Phi}_2$ to the wing surface as part of the incidence correction to $\tilde{\Phi}_0$, whereas the second term $\epsilon\Theta\hat{C}'\tilde{\Phi}_1$ accounts for the 3-D compressibility correction to the PDE without altering the wing boundary condition.

The PDE for $\tilde{\Phi}_0$ is the same as that for $\hat{\Phi}_0$ with $\tilde{x}$ and $\tilde{z}$ replacing $\hat{x}$ and $\hat{z}$; the linear PDE governing $\tilde{\Phi}_1$ obtained from Eq. (3.11) is

$$\left\{\left[K_n - (\gamma+1)\tilde{\Phi}_{0\tilde{x}}\right]\frac{\partial^2}{\partial\tilde{x}^2} + \frac{\partial^2}{\partial\tilde{z}^2} - (\gamma+1)\tilde{\Phi}_{0\tilde{x}\tilde{x}}\frac{\partial}{\partial\tilde{x}}\right\}\tilde{\Phi}_1 \\ = -2\left(\tilde{x}\frac{\partial}{\partial\tilde{x}} + \tilde{z}\frac{\partial}{\partial\tilde{z}}\right)\tilde{\Phi}_{0\tilde{x}}. \qquad (3.21)$$

where the right-hand member results because $\hat{\Phi}_{0\hat{x}} = \tilde{\Phi}_{0\tilde{x}}$ and $\partial/\partial\hat{y} = \sec\Lambda\,\partial/\partial\tilde{y} - (\hat{C}'/\hat{c})(\tilde{x}\frac{\partial}{\partial\tilde{x}} + \tilde{z}\frac{\partial}{\partial\tilde{z}})$. The $\tilde{\Phi}_2$ satisfies the homogeneous part of Eq. (3.21). On the wing portion of the x-axis ($\tilde{z} = \pm 0$), $\partial\tilde{x}_0/\partial\tilde{z} = d\tilde{Z}^{\pm}/d\tilde{x}$, $\partial\tilde{\Phi}_1/\partial\tilde{z} = 0$, and $\partial\tilde{\Phi}_2/\partial\tilde{z} = 1$. The jump conditions for a shock, if it exists, must be derived from Eqs. (3.12), not from the jump conditions for the weak solutions to Eq. (3.21). Since $\hat{\Phi}_0 \equiv \hat{c}\tilde{\Phi}_0$, and $\hat{\Phi}_1 = \epsilon\Theta\hat{c}\hat{C}'\tilde{\Phi}_0 - \epsilon\sqrt{K_n}\tilde{C}_1^i\hat{c}\tilde{z} + \\ + \epsilon\left[\sqrt{K_n}\tilde{C}_1^i + \hat{I} + \Theta\tilde{Z}_0'\right]\hat{c}\tilde{\Phi}_2$, the conditions in question can be deduced from Eq. (3.12), to be applied at the unperturbed shock boundary $\tilde{x} = \tilde{x}_0^D(\tilde{z})$. We give below the conditions for $\tilde{\Phi}_1$,

$$(\gamma+1)\left\langle\tilde{\Phi}_{1\tilde{x}} + \tilde{x}_1^D\tilde{\Phi}_{0\tilde{x}\tilde{x}}\right\rangle - 2(\tilde{x}_0^D)'(\tilde{x}_1^D)' = 2\tilde{x}_0^D, \qquad (3.22a)$$

$$\left[\!\left[\tilde{\Phi}_{1\tilde{x}} + \tilde{x}_1^D\tilde{\Phi}_{0\tilde{x}\tilde{x}}\right]\!\right] = 0. \qquad (3.22b)$$

The far-field behavior of $\tilde{\Phi}_0$, $\tilde{\Phi}_1$, and $\tilde{\Phi}_2$ can be developed from their governing PDEs and will be given below more fully than Eq. (3.13), inasmuch as they are explicitly used on the far boundary in the computation work discussed in § 5. Here, for large $\tilde{\zeta} \equiv \tilde{x} + i\sqrt{K_n}\,\tilde{z}$,

$$\tilde{\Phi}_0 \sim \frac{\tilde{\Pi}_0}{2\pi}\tilde{\theta} + \left(\tilde{D}_0^r\tilde{x} - \tilde{D}_0^i\sqrt{K_n}\,\tilde{z}\right)/|\tilde{\zeta}|^2 + \\ + \frac{\gamma+1}{4K_n}\left(\frac{\tilde{\Pi}_0}{2\pi}\right)^2\left[\ln|\tilde{\zeta}| + K_n\tilde{z}^2/|\tilde{\zeta}|^2\right]\tilde{x}/|\tilde{\zeta}|^2, \qquad (3.23a)$$

$$\tilde{\Phi}_1 \sim \frac{\tilde{z}}{\sqrt{K_n}}\frac{\tilde{\Pi}_0}{2\pi}\ln|\tilde{\zeta}| + \frac{\gamma+1}{8\pi K_n^2}\left(\frac{\tilde{\Pi}_0}{2\pi}\right)^2\left\{2\left(\ln|\tilde{\zeta}|\right)^2 + \right. \\ \left. + 2\frac{\tilde{x}^2 - K_n\tilde{z}^2}{|\tilde{\zeta}|^2}\ln|\tilde{\zeta}| - \frac{1}{2}\frac{(\tilde{x}^2 - K_n\tilde{z}^2)^2 - 4K_n\tilde{z}^2\tilde{x}^2}{|\tilde{\zeta}|^4}\right\} + \\ + \frac{\tilde{\Pi}_1}{2\pi}\ln|\tilde{\zeta}| + \frac{\tilde{\Pi}_0}{2\pi}\tilde{\theta} - \frac{2}{\sqrt{K_n}}\left(\tilde{D}_0^i\tilde{x} - \tilde{D}_0^r\sqrt{K_n}\,\tilde{z}\right)\tilde{z}/|\tilde{\zeta}|^2 \qquad (3.23b)$$

$$\tilde{\Phi}_2 \sim \frac{\tilde{\Pi}_1}{2\pi}\tilde{\theta} + \frac{\gamma+1}{8\pi^2K_n^2}\tilde{\Pi}_0\tilde{\Pi}_2\left[\ln|\tilde{\zeta}| + \right. \\ \left. + K_n\tilde{z}^2/|\tilde{\zeta}|^2\right]\tilde{x}/|\tilde{\zeta}|^2, \qquad (3.23c)$$

where $\tilde{\theta} \equiv \tan^{-1}(\tilde{x}/\sqrt{K_n}\,\tilde{z}) + \frac{\pi}{2}\operatorname{Sgn}\tilde{z}$. These results are completely recoverable from the corresponding results for $\hat{\Phi}_0$ and $\hat{\Phi}$, in the more general case, after observing $\tilde{\Pi}_0 = \hat{c}^2\hat{\Pi}_0$, $\tilde{D}_0^i = \hat{c}^2\hat{D}_0^i$, $\tilde{D}_0^r = \hat{D}_0^r\hat{c}^2 - (\gamma+1)(16K_n)^{-1}(\hat{\Pi}_0/\pi)^2\ln\hat{c}$, $\tilde{d}_1 = \Theta\hat{c}^2\hat{d}_1 - (\gamma+1)(8\pi K_n)^{-1}(\hat{\Pi}_0/\pi)^2\ln\hat{c}$, etc. Note in particular that, unlike $\tilde{\Phi}_1$ in Eq. (3.13b), the upwash contribution $\sqrt{K_n}\,\tilde{C}_1^i\tilde{z}$ appears in neither $\tilde{\Phi}_1$ nor $\tilde{\Phi}_2$, and that $\tilde{\Pi}_0$, $\tilde{\Pi}_1$, $\tilde{\Pi}_2$, $\tilde{D}_0^r$, $\tilde{D}_0^i$, etc. are pure constants.

The upwash effect now appears as an incidence correction $\sqrt{K_n}\,\tilde{C}_1^i$ in the reduced problem and is determined from

$$\sqrt{K_n}\,\tilde{C}_1^i = \sqrt{K_n}\,\hat{C}_1^i - \frac{\Theta}{2\sqrt{K_n}}\frac{\hat{\Pi}_0}{\pi}\hat{C}'\ln\hat{c} \qquad (3.24)$$

with $\sqrt{K_n}\,\hat{C}_1^i$ evaluated from Eq. (3.17). The source strength can be determined with the help of Green's Theorem; for the system with similarity structure considered, $\tilde{Q}_1$ can be explicitly evaluated from[14]

$$\tilde{Q}_1 = \frac{4\pi}{K_n}\tilde{D}_0^r + \frac{\gamma+1}{8\pi K_n^2}\tilde{\Pi}_0^2\left[3 + \tilde{a} + (\tilde{a}+\tilde{b})^2\right]$$

where $\tilde{a}$ and $\tilde{b}$ are the leading and trailing edge locations in $\tilde{x}$, respectively.

3.8 An Unsteady Analogy

For wings with sections profile not being generated from a single shape, the greatly simplified solution procedure based on the similarity structure discussed in § 3.7 is not applicable. An unsteady analogy exists, however, which provides an alternative, and perhaps numerically more effective, solution procedure for the inner problem in the more general case.

Let

$$\hat{\tau} \equiv \hat{y}/\epsilon\Theta, \quad \varphi \equiv \hat{\Phi} + \epsilon\sqrt{K_n}\,\hat{C}_1^i\hat{z}, \qquad (3.25a,b)$$

the PDE (3.4) then appears as

$$\frac{\partial}{\partial\hat{x}}\left(K_n\varphi_{\hat{x}} - \frac{\gamma+1}{2}\varphi_{\hat{x}}^2\right) + \varphi_{\hat{z}\hat{z}} = 2\varphi_{\hat{x}\hat{\tau}}. \qquad (3.26)$$

This is a familiar form in the analysis of unsteady transonic small-disturbance flow in the nonlinear regime[48, 49]. The wing boundary condition Eq. (3.7) now reads

$$\left(\frac{\partial\varphi}{\partial\hat{z}}\right)_w = \frac{\partial\hat{Z}^{\pm}}{\partial\hat{x}} + \frac{d\hat{Z}_0}{d\hat{\tau}} + \epsilon\left(\hat{I} + \sqrt{K_n}\,\hat{C}_1^i\right), \qquad (3.27)$$

to be applied at $\hat{z} = \pm 0$, $\hat{a}(\hat{\tau}) < \hat{x} < \hat{b}(\hat{\tau})$. Thus, an analogy of the inner problem for $\hat{\Phi}$ with an unsteady 2-D transonic airfoil problem exists, in which, since $\epsilon\Theta$ is small, the unsteady motion is confined to the neighborhood of the quasi-steady limit. The crucial input to such an unsteady problem is of course, the incidence correction $\epsilon\sqrt{K_n}\cdot\hat{C}_1^i(\hat{\tau})$ which is a functional of $\hat{\Pi}_0(\hat{\tau})$; the latter can be replaced by an approximate distribution

from a solution of Eq. (3.26), with $\sqrt{K_\infty}\,\hat{C}_i^{\,i}$ set equal to zero in Eq. (3.27). With the ADI algorithm (49), this approach promises an effective computational procedure, especially in capturing shocks and in avoiding the ambiguity associated with the reexpansion singularity at the shock root as well as the problem with a very weak shock (discussed in § 4.3).

Numerical results have been obtained for oblique wings via this approach in an unpublished work by T. Evans and the senior author, and compare reasonably well with those obtained from the local-similarity solutions. Some of Evans' nonlifting examples have been discussed in Ref. 14 (b).

4. LIMITATIONS AND COMMENTS ON THE THEORY

The asymptotic nature of the analysis not only restricts the application mainly to high-aspect-ratio wings, but also lead to a number of nonuniformities, i.e. regions of local breakdowns, which limit considerably the usefulness of the theory. There has also been questions raised on the uniqueness and existence of solutions to the reduced problems. Comments on these and other questions are given below.

4.1 The Uniqueness Problem and Shock-Free Supercritical Airfoil

The existence and uniqueness of the reduced problem for $\hat{\phi}_0$ is, of course, the same in the 2-D TSD theory[40, 50, 51]. For the uniqueness of the 3-D correction $\epsilon\hat{\phi}$, the problem may be considered being equivalent to asking whether the homogeneous part of PDE (3.4) has a solution $\hat{\phi}, \neq 0$, with $(\partial\hat{\phi}/\partial\hat{z})_w = 0$. It is essential to point out that the swept and unswept wings, as well as the 2-D airfoil, share the same uniqueness problem mentioned, since the 3-D influence enters only as a nonhomogeneous term in their equations. Thus the uniqueness proof given by Cook[16] for the lifting-line theory of the straight, unyawed wings in transonic flow should also be applicable to the swept-wing case. [The idea in Cook's proof runs parallel to Morawetz's earlier work on 2-D mixed-flow in the hodograph plane[52], but differs from Morawetz's in the use of the physical plane and in allowing circulation.]

Two important questions arise concerning the analysis in which $\hat{\phi}_0$ represents a shock-free supercritical (component) flow: (i) can a shock-free perturbation $\epsilon\hat{\phi}$, exist? (ii) How should the shock be treated in an asymptotic theory for small ϵ in this case, if $\epsilon\hat{\phi}$, is not shock-free? Definitive answers to these questions are not available to date. In fact, the proof given by Cook[16] aims chiefly at proving uniqueness for the perturbation of a shock-free supercritical solution $\hat{\phi}_0$, with the implicit assumption that the perturbation solution $\epsilon\hat{\phi}$, will exist.*

* One must recall that the significance of Morawetz's original uniqueness study was concerned with the question of existence [53], where she found that, to maintain an imbedded shock-free supercritical flow, the airfoil profile variation, say $\tilde{z} = \tau f(\tilde{x})$, cannot be arbitrarily prescribed on a portion of surface containing the maximum-velocity point, with the exception of certain very special distribution of $f(\tilde{x})$. Cook's implicit assumption then would amount to the stipulation that $f(\tilde{x})=\tilde{x}$!

In passing, we may remark that, if a 2-D shock-free supercritical profile were to be used in the 3-D wing design, the unswept (straight) wing appears to posess one advantage, (although there are other obvious drawbacks) since the nonhomogeneous terms of the PDE (3.4) vanishes in this case, and the remaining 3-D effect can be eliminated by a proper twist distribution

$$\hat{I}(\hat{y}) = -\sqrt{K_\infty}\,\hat{C}_i^{\,i}(\hat{y}) \tag{4.1}$$

[Of course, this condition can be useful also to the oblique and swept wings, since the contribution from the other correction, i.e. the 3-D compressibility effect, is relatively small in magnitude in many cases.]

4.2 Breakdown Near the Leading Edge

The breakdown of the asymptotic analysis of § 3 can be separated into two categories. One arises mainly from a small-disturbance approximation which must fail in the vicinity of a stagnation point, or where the $\hat{x}$-gradient is singular; the other category associates more directly with the high-aspect-ratio expansion, in which the spanwise gradient is assumed to be small and must fail where $\partial\hat{\phi}/\partial\hat{z}$ is singular. The nonuniformity of the second category will be examined in §4.3.

Stagnation points occur near both leading and trailing edges, the problem is less serious with a sharp trailing edge since with the Kutta condition, the region of this breakdown is exponentially small, as is well known. For an airfoil with a leading-edge radius comparable to $\tau^2 C_\phi$, $\hat{Z}^{\pm}$ is proportional to $(\hat{x}-\hat{a})^{1/2}$ near the leading edge and the TSD theory[53, 54] gives an infinite $(\hat{\phi}_0)_{\hat{x}}$ like $(\hat{x}-\hat{a})^{-1/3}$. The same behavior remains, in fact, even if the camber, or absolute incidence, is comparable to the thickness[55]. The region where $\alpha^{2/3}\hat{\phi}_{0\hat{x}}$ becomes comparable with unity is

$$\hat{x}-\hat{a} = O(\alpha^3) = O(\epsilon^6), \tag{4.2}$$

indicating that the leading-edge singularity will not affect the usefulness of the theory until one reaches the nose region which is $\hat{x}-\hat{a} = 0\ (\tau^2)$, since $\tau = O(\alpha)$ here.

It may be pointed out that the magnitude of the drag coefficient contributed by the surface pressure in 2-D is of the order τ^{-} (of which a nonvanishing portion is contributed by the singular pressure coefficient near the nose region), while the stagnation region at the nose contributes to a smaller leading-edge force comparable to τ^2, i.e. α^2. The latter is exactly an order ϵ higher than $\tau^{5/3}$ and, therefore, is essential if the 3-D effect on the transonic drag rise is to be consistently analyzed. For this reason, a development of the lifting-line theory on the basis of the potential equation without the small-disturbance assumption appear to be worthwhile[56]. Additional reasons favoring the use of a full potential equation are given later in § 5.

4.3 Nonuniformity Near a Shock Root

For flow with an imbedded supercritical

region terminating by a shock, the reexpanding supersonic flow develops a weak singularity at the shock root (the intersection of the shock and an impermeable surface), unless the surface has a zero curvature, as is well known[57]. In particular, the fluid tangential velocity behaves as

$$(\hat{u}-\hat{u}_{sr})/\|\hat{u}\|_{sr} \sim R.P.\left[\frac{4}{\pi}\ln(\zeta/\kappa_1)-i\zeta\right] \qquad (4.3a)$$

where $\hat{u}\equiv\hat{\phi}_{\hat{x}\hat{x}}$, the subscript "$sr$" refers to the shock root and $\zeta\equiv\xi+i\eta$; ξ and η are rescaled coordinates with the origin at the shock root:

$$\left.\begin{aligned}\xi &\equiv \hat{Z}''_{sr}\left(\frac{\gamma+1}{2}\right)^{-1/2}\left|\|\hat{u}\|_{sr}\right|^{-3/2}\cdot(\hat{x}-\hat{x}_{sr})\\ \eta &\equiv \hat{Z}''_{sr}\left|\|\hat{u}\|_{sr}\right|^{-1}\cdot\hat{z}\end{aligned}\right\} \qquad (4.3b)$$

In above $\hat{Z}''\equiv\partial^2\hat{Z}/\partial\hat{x}^2$ is proportional to the surface curvature and κ_1 is a constant determined by the surrounding flow. It follows that $\hat{u}_{\hat{x}\hat{x}}=\partial^3\hat{\phi}_0/\partial\hat{x}^3$ becomes infinity at the shock root ($\xi=0$) like $\ln|\xi|$, leading to a logarithmically infinite shock jump for $\epsilon\,\partial\hat{\phi}_1/\partial\hat{x}$ at the shock root, (cf. Eq. (3.12a)). Although, one may argue that this rather weak singularity would affect little the lift, moment as well as drag, the failure to yield a correct (finite) pressure jump at the surface appears to have defeated one of the original purposes for analysing the shock perturbation.

However, this local breakdown can be treated (14b), once if it is realized that the form of the reexpansion singularity in $\hat{u}$ (not in $\hat{\phi}$) given in Eq. (4.3) is unaffected by the presence of the 3-D compressibility correction $\epsilon^2\hat{\phi}_{\hat{y}\hat{y}}$ in the composite PDE (3.4). Thus any 3-D (or the analogous unsteady) influence on the local structure of the $\hat{\phi}_{\hat{x}}$, or pressure field, can result only through changes in the three constants $\|\hat{u}\|_{sr}$, $\hat{x}_{sr}$, and κ_1. In fact, by expanding $\hat{u}_{sr}$, $\hat{x}_{sr}$ and κ_1 in small ϵ for fixed $\hat{x}$ and $\hat{z}$ (appropriate at points far from the shock root), one recovers from Eq. (4.3a) the logarithmic singularity in the previous expansion. Furthermore, matching this with the singular solution to $\hat{\phi}=\hat{\phi}_0+\epsilon\hat{\phi}_1+\cdots$ permits the determination of the corrected values for the shock jump and for the shock-root location.

Implicit in the formulation involving shocks in § 3 is that $\epsilon\|\hat{\phi}_{\hat{x}}\|$ is small relative to $\|\hat{\phi}_{0\hat{x}}\|$. This condition is not realized where the shock strength approaches zero. At least for solutions constructed from the similarity structure (§ 3.7), in which the shock jump is controlled explicitly by $\epsilon\,d\bar{C}/d\bar{y}$, (weak) unrealistic expansion snock may appear from such an analysis (if the 2-D solution for the component flow has a weak shock). However, the inner solutions based on the composite PDE (3.4), or on PDE (3.26) for the unsteady analogy, will not encounter this difficulty. Comparison of the similarity solution with that based on the unsteady analogy for the case involving weak snocks is therefore valuable.

4.4 Nonuniformities at Wing Tips and at the Apex

As made apparent in § 2.3, the analysis given in §§ 2 and 3, without further refinement, will breakdown at a distance

$$\bar{y}\pm 1 = O(\epsilon^2\ln\epsilon) \qquad (4.4)$$

from the tips, and at a distance

$$\bar{y} = O(\epsilon) \qquad (4.5)$$

from the apex of a swept wing. Implicit in Eq. (4.4) is the assumption that the span load computed from $\bar{\gamma}_0$ (i.e. from the strip theory) vanishes at the tip like an elliptic load (cf. Fig. 6a). For an untwisted tapered wing, or one with a square tip (cf. Fig.s 6b and 6c), we infer that, instead of Eq. (4.4), the nonuniformity in this case occurs at

$$\bar{y}\pm 1 = O(\epsilon). \qquad (4.6)$$

This follows from the last integral of Eq. (2.6c), which, when interpreted in Stieltjes' sense, gives the additional terms (for $\bar{y}\to 0$)

$$\frac{\bar{\Gamma}_0(1)}{1-\bar{y}}\left[1-\sin\Lambda(1)\right] + \frac{\bar{\Gamma}_0(-1)}{1+\bar{y}}\left[1+\sin\Lambda(-1)\right] \qquad (4.7)$$

A comparison of the present solutions with more exact numerical analyses for the cases involving untwisted tapered swept (or oblique) wings and for the swept wings with an apex, should be helpful in assessing the extent to which these nonuniformities affect the usefulness of the analysis.

It may be pointed out that the flow field next to the apex must, in any practical situation, be modified by the presence of a (slender) fuselage; therefore, the solution breakdown near $\bar{y}=0$ should not be a serious practical concern, and may presumably be separately treated. The relatively small scale in $\bar{y}$ or $(\bar{y}\pm 1)$ indicated by Eq. (4.4) - (4.6) suggests that the equation governing the regions around the apex and the tips to be reanalyzed is the 3-D TSD equation (noting that $\epsilon\equiv\alpha^{1/3}c/2b$). These extensions remain to be investigated.

5. COMPUTATIONS: EXAMPLES AND COMPARISIONS WITH FULL POTENTIAL SOLUTIONS

Inasmuch as the existence and uniqueness of the solutions cannot be easily investigated, demonstration of numerical solutions to the reduced problem is an essential part of the study. The theory has been limited by the assumptions of a high-aspect-ratio and of the small disturbance; it is uncertain that the analysis may predict the aerodynamic characteristics for swept wings to the same degree enjoyed by the lifting-line theory for the straight unyawed wings. In view of this, and the several nonuniformities of the analysis discussed in the preceding section, we consider the direction comparison with the more exact, 3-D full potential solution an integral part of this research. Before going on to the discussion of the computations, some remarks will be made on the basis of the more exact potential-flow computation programs which are involved in the comparison study.

5.1 Remarks on Existing 3-D Potential Computer Code

The unrefined nature of the far-field description in most discretized flow-field computation methods, as a result of the computer storage and

computation time limitations, is well known. This problem becomes more serious in the 3-D cases (20-24). It is not at all clear from the published data whether the grid distributions used therein are sufficiently refined for the purpose of describing adequately the upwash induced by the far-wake vorticities, which has been so crucial to the analysis of a high-aspect-ratio wing.

There appears to be an additional problem brought about by the scarcity of the span stations available in the current 3-D transonic program (21-24). In the FLO 22 code for planar wings(22) a total of twenty-one (21) span stations are allowed. Applying it to an oblique wing, for example, there remains only ten (10) stations on each wing panel, and one certainly cannot attach too much confidence to the results obtained for the tip region in this case. It has also been known among users that the span load and sectional lift coefficient so obtained are far from being very smooth--the values at successive stations appears to alternate noticeably about some mean curve. Fig. 7 shows typical results of sectional lift coefficient obtained from the converged solutions generated from two versions of the FLO 22 code for an elliptic wing pivoted at 30° at $M_\infty = 0.755$. Except for this limited, but noticeable, irregularity in the transonic-speed range which require some caution in making a comparison with the asymptotic analysis the method is known to be capable of reproducing the span loads determined by the (linear) panel methods for the subsonic speed range(58).

Presumably, this irregularity has not been observed in the 3-D computations using the transonic small-disturbance equation(20). We may point out however that the current 3-D TSD codes are not applicable directly to problems lacking a bi-lateral symmetry such as that of an oblique wing. Furthermore, the small-disturbance assumption breaks down near the leading edge, comparison with TSD code will not reveal one of the important limitations of the present (transonic) theory. For the two above reasons, comparison with the TSD codes has not been made. We believe such a comparison can be quite useful in our future study focusing on shock-wave patterns.

From a strict theoretical view point, the most serious limitations of current 3-D full-potential codes is the empiricism introduced by modelling the inviscid wake in the formulation, which we believe is unnecessary. Two assumptions were introduced in Refs. 21-24: (i) the shape of the trailing vortex (TV) sheet is specified a priori; (ii) a condition equivalent to (in the present notations)

$$\phi_{zz} = 0 \qquad (5.1)$$

is applied at the TV sheet. Assuming a thin airfoil section, assumption (i) is seen to be equivalent to that in the TSD theory, with the TV sheet transferred to the "wing trace" on the x-axis. The condition (ii) is incorrect, strictly speaking, and requires a clarification†. Were Eq. (5.1) to hold on both sides of the sheet, Refs. 22-24 would imply that the PDE at far-downstream should yield (in the present notations)

$$[\![\phi_{\tilde{z}}]\!]_{TV} = 0 \quad \text{or} \quad \phi^+_{\tilde{z}} = \phi^-_{\tilde{z}} \qquad (5.3)$$

that is, the upwash is continuous across the sheet or the trace. This and the continuity of $\phi_{\tilde{x}}$ are then the correct TV-sheet condition, which is at least consistent with the small-disturbance theory. On the other hand, the programs similar to those in Refs. 22-24 do lead to results consistent with experimental data. This can be reconciled by the observation that if we were to stipulate the incorrect assumption of continuity in $\phi_{\tilde{z}\tilde{z}}$, then Eq. (5.3) would become consistent with $\phi_{\tilde{z}\tilde{z}} = 0$. It is apparent that in the difference equations of Ref. 22-24, Eq. (5.3), but not Eq. (5.1), was actually used. We may conclude that while $\phi_{\tilde{z}\tilde{z}} = 0$ appears to be erroneous, the code actually uses the more appropriate condition Eq. (5.3), and that the wake-modelling in Ref. 21-24 introduces an error comparable to that in the small-disturbance theory.

5.2 Computations of $\tilde{\phi}_0$, $\tilde{\phi}_1$, and $\tilde{\phi}_2$

The reduced mixed-type problems for the $\tilde{\phi}_0$, $\tilde{\phi}_1$, and $\tilde{\phi}_2$ in the similarity solutions (§ 3.7) are solved numerically by a relaxation method, using type-sensitive difference operators corresponding to Murman's "fully conservative form"(50). The procedure of line relaxation used for $\tilde{\phi}_0$ may be considered standard, except for the uses of an improved far-field description with Eq. (3.23a)+ and of a third-order convergence acceleration scheme(60). Shock fitting algorithm(61) is being used in conjunction with the shock perturbation analysis based on Eq. (3.22) for $\tilde{\phi}_1$, and similar treatment for $\tilde{\phi}_2$, but will not be discussed here, inasmuch as the cases with subcritical, and slightly supercritical, component flow studied below in § 5.3 are shock-free.

For $\tilde{\phi}_1$, and $\tilde{\phi}_2$, the problems are linear and the transition and/or shock-jump boundaries are known from the $\tilde{\phi}_0$ solution, but they require a greater storage owing to the variable coefficients. A nonuniform mesh with 81 x 61 grid points over a computation domain $|\tilde{x}| \lesssim 6$, $|\tilde{z}| \lesssim 6$, were used by Cheng and Meng(13,14) ($\Delta\tilde{x}$ is uniform over the wing section). A subsequent program employs three successive grid-halvings up to a mesh of 124 x 92 (with nonuniform $\Delta\tilde{x}$ on the wing). The leading and trailing edges are located at $\tilde{x} = -1$ and $\tilde{x} = +1$, respectively (i.e. $-\tilde{a} = \tilde{b} = 1$); a departure of "$\tilde{a}$" from negative one can be accounted for by changing all $\tilde{x}$ to $(\tilde{x} + 1 + a)$ in the equations governing the similarity solutions. The case $-\tilde{a} = \tilde{b} = 1$ corresponds to a swept, or oblique, wing with the straight axis $\tilde{x} = 0$ coinciding with the 50% chord line.

The iterative solutions in Refs. 13 and 14 uses uses a relaxation factor of 1.8 and 0.8 in the elliptic and hyperbolic region, respectively; 200-300 sweeps are needed for convergence of the circulation to within 10^{-5}. On an IBM 3031, using double-precision arithmetics, the convergenced solution for each $\tilde{\phi}_i$ requires typically 10-12 minutes.* We note in passing that a computer

† This controversial condition was brought to my attention by Dr. Norman D. Malmuth.

+ A 2-5% change in surface pressure results from the improvement in the far-field description based on Eq. (3.23a).

* The IBM 3031 at the University of Southern California Campus has an expandable core memory of 300-6400 K words.

program similar to that for $\tilde{\phi}_2$ has been considered in the context of a straight unyawed wing by Small[17].

5.3 Examples: Comparison with Solutions Based on the Full-Potential PDE

For the expressed purpose of comparing the asymptotic analysis (the similarity-solution structure in particular) with the corresponding full-potential solutions, we consider below examples of oblique as well as symmetric swept wings with high subcritical and slightly supercritical component flows. All wing planforms considered are elliptic, with the major axis coinciding with the mid (50%) chord; the wing sections are generated from a single profile NASA 3612-02, 40, rescaled to an arbitrary thickness τ. The latter will be set equal to α in the theory. These wings fulfill the geometrical description of Eq. (3.18) and, therefore, the inner solution can be obtained by a linear combination of the basic similarity solutions $\tilde{\phi}_0$, $\tilde{\phi}_1$, and $\tilde{\phi}_2$, which will be determined after specifying the component transonic parameters K_n, the incidence, and the locations of the leading and trailing edges. We pointed out that the airfoil profile considered has been used in various wind tunnels and preliminary design studies of oblique wings at M = 0.60 - 1.4[4,62]. Several sets of these basic similarity solutions have been obtained for $K_n = 3.6$ and $K_n = 3.45$, and have been described in some detail in Refs. 13 and 14. These solutions are used in the subsequent comparison with the full potential solutions.

To illustrate the solutions' behavior, we show the surface distributions of $\tilde{\theta}_{0\bar{x}}$, $\tilde{\theta}_{1\bar{x}}$, and $\tilde{\theta}_{2\bar{x}}$ in Fig. 9, for zero incidence and Kn = 3.45. The basic component flow, for the $\tilde{\theta}_{0\bar{x}}$ shown in Fig. 9 is slightly supercritical. The critical condition for the 2-D component in this case is $\tilde{\theta}_{0\bar{x}} = K_n/(\gamma+1) = 1.438$.

Numerical results comparable with our solutions are generated from one version of A. Jameson's 3-D full-potential computer codes "FLO 22" (See Refs. 6,21), which is used with implementations for oblique-wing analyses at NASA Ames Research Center Aeronautics Division and at Grumman Aerospace Corporation Research Department. The algorithms employed in FLO 22 are not fully conservative, but this may not be essential for shock-free solutions presented below. We point out that the FLO 22 data from NASA Ames and from Grumman are not identical, owing mainly to the use of different meshes. The availability of data from two sources is helpful in delineating the nature of discrepancy between our theory and the more exact 3-D programs as noted in §5.1. Data from the latter is still influenced by the mesh size, spacing of the span stations, number of iterations, the detail of the leading-edge geometry description, which are different in the NASA Ames and the Grumman calculations.

A number of FLO 22 runs have been made for the oblique wings with free-stream Mach number, swept angle, wing-thickness, etc. chosen to give either $K_n = 3.6$ or $K_n = 3.45$ employing the same basic airfoil section. An elliptic planform is used in each case; wing twist and wing bend are assumed to be zero, as noted earlier. Among the first comparison studies made is a case with relatively thin wing section (6% thickness ratio) and a rather high aspect ratio (an elliptic planform with a major-to-minor axes ratio of 20). The surface pressure coefficients in this case have been presented in the journal paper (Ref. 14a), we consolidated them here in a single plot (Fig. 9) in order to show differences from the subsequent comparisons involving considerably thicker wing sections and larger sweep angles. The free-stream Mach number and the sweep angle used in the FLO 22 calculation is $M_\infty = 0.8242$ and $\Lambda = 22.5°$, giving a component Mach number $M_n = 0.7615$. Thus, we have $K_n = 3.60$, $\mathcal{D} = 1.003$ and $\epsilon = 0.1277$ in this case; the component flow is slightly below being critical. The FLO 22 data from NASA Ames (in small crosses and "v") and from Grumman (in small open circles) shown in the plot appear to be rather close except next to the leading edge. The Cp values computed from the similarity solution (shown in solid curves) agree reasonably well with the FLO 22 data except near the leading edge, as anticipated.

Encouraging is that the degree of agreement with the FLO 22 data does not appear to deteriorate much with increasing the wing thickness, or reducing the wing aspect ratio. The consolidated plot in Fig. 10 shows the surface pressure coefficient at seven span stations on a 12% thick, 14:1 elliptic wing, pivoted at $\Lambda = 30°$ for $M_\infty = 0.7677$. The component Mach number is $M_n = 0.6648$ in this case, giving $K_n = 3.45$. The three sets of surface data of Fig. 8 are used to construct the Cp distributions shown in heavy solid curves. The Cp value for the component flow is -0.689 in this case and both solutions give the appearance of supercritical shock-free regions on the upper surface of the downstream wing panel.

The agreement between the FLO 22 data and those based on the asymptotic analysis in both Figs. 9 and 10, should be considered as being better than expected, inasmuch as the relative error in the asymptotic theory belongs to an order determined by $\epsilon^{2/3}$ or ϵ^2, which ever is larger. The magnitudes of $\epsilon^{2/3}$ for the examples shown in Fig. 9 and Fig. 10, are, respectively, $\epsilon^{2/3} = 0.153$ and 0.243. It may be recalled that there is a noticeable difference between the two sets of FLO 22 data shown in Fig. 7. The agreement found here appears to add credence to the Ames data set in this case.

It is not altogether clear that the encouraging agreement found for the pivoted wings may still hold to some degree with the presence of an apex in a symmetric swept wing. Figure 11 presents a consolidated plot for surface pressure coefficient at seven span stations on a symmetric swept wing with the same basic (elliptic) planform, sweep angle, and section profile as those in the preceding figure. The free-stream Mach number is however, lower with $M_\infty = 0.7549$; thus, $M_n = 0.6538$, $K_n = 3.60$, $\epsilon = 0.1448$ and $\mathcal{D} = 1.062$. The solution remains subcritical for most stations, component-wise. The stations $\bar{y} = 0.92$ and 0.97 are included

*In both the asymptotic analysis and the FLO 22 calculation, the wing sections are taken to be perpendicular to the straight axis, therefore, the sectional cuts shown in Fig. 10 are graphically incorrect. The differences resulting from changing the orientation of the cuts turns out to be numerically small, however.

to illustrate the manner in which the solutions behave near the tip, where the trends of departure of the asymptotic from the FLO 22 analyses, as well as between the two sets of FLO 22 data themselves, are clearly evident. Away from the tip, agreement is as reasonable as in the two preceding comparisons for the oblique wings. However, the set of FLO 22 data in filled circles (black dots) gives a consistently higher peak for -Cp than the one in open circles. The discrepancy may be explained by the uncertainty associated with the fluctuating spanwise distributions of sectional lift shown in Fig. 7. The asymptotic analysis tends to give a consistently lower -Cp than the FLO 22 data on the lower surface around the quarter chord. This tendency is also apparent from Fig. 10. This small but noticeable discrepancy may be associated with the accuracy and degree of convergence in the $\bar{\phi}_0$ solution. Results obtained most recently for $\bar{\phi}_0$ based on a more refined mesh and with a small residue appears to alter the Cp values on the lower surface slightly in the right direction.

The most important piece of information from Fig 11 is the comparison made for the station closest to the apex. At 10% semi-span from the symmetry plane ($\bar{y} = 0.097$), the agreement of the asymptotic results with the FLO 22 data (in open circles) remain as good as other stations. Even for the FLO 22 data belonging to the second set (black dots), the agreement with the results is on the similarity solution is still reasonable.

6. CONCLUDING REMARKS

The foregoing presentation has shown that Prandtl's lifting-line idea, originally applied to an unyawed, straight wing of high aspect ratio, can be extended to the study of 3-D mixed flows over transonic swept wings. Examples of oblique (pivoted) and symmetric swept wings involving high subcritical and supercritical component flows are shown; comparisons with full-potential solutions from existing codes are made. Except near the wing tip and the wing root, and also the leading edge, where breakdowns are expected; the agreement with the full-potential results is encouraging.

A salient feature brought out by the asymptotic analysis is a contribution to the upwash correction proportional to $\epsilon \ln \epsilon \, d\bar{\Gamma}/d\bar{y}$, resulting from the spanwise (y'-) component of the locally shedded wake vorticities, even though the latter's effect on the other velocity component is relatively small (in the transonic regime considered). The dependence of the upwash correction on the sweep and on the span loading have been shown; the explicit result presented in § 2.1 should be quite useful for controlling the 3-D effects on the transonic component flow in design studies. Another essential ingredient of the analysis, absent in the classical theory, is a source-like compressibility correction to the PDE of the component flow; it leads to a line-source effect in the outer flow.

An important gain in the theoretical development through this approach is the availability of a similitude in the 3-D flow structure (§3.7), applicable to wings with sections generated from a single profile. With the similarity solutions, the reduced 2-D problems can be solved once for all span stations; the explicit dependence of the flow field on wing sweep, aspect ratio, and spanwise distribution of the local chord, as well as twist and bend, can be studied.

The examples analyzed thus far do not include cases with imbedded shocks. Solutions making use of the 3-D corrections for the shock jump and the shock geometry (§§3.3 and 3.7) and of the treatment of the re-expansion nonuniformity (§ 4.3), remain to be demonstrated. In this paper, we have not discussed the computational study based on the unsteady analogy (§ 3.8), yet to be completed. Unpublished results computed from this analogy with an ADI algorithm by Evans compare rather closely with similarity solutions and promise an effective procedure for treating complicated shock patterns.

Whereas a localized treatment of the leading-edge breakdown is possible, a solution to this difficulty is to develop a lifting-line theory on the basis of the potential theory without the small-disturbance assumption. A work along this line has already been carried out in Ref. 58, where, interestingly, solutions via similarity flow structure may again be found. As noted earlier, in (§2.1), the inner solution in such a formulation should provide a proper treatment of the vortex-sheet geometry near the trailing edge, unaccounted for in most (if not all) current 3-D computer codes. Treatment of nonuniformities at the root and the tip sides are the remaining problems for the lifting-line theory; their analyses for the transonic regime, as observed in (§4.4), would involve solving a fuller 3-D problem.

ACKNOWLEDGEMENT

The material in this paper is taken largely from studies performed at the University of Southern California and supported by the Office of Naval Research, Fluid Dynamics Program (Contract N00014-75-C-0520) as well as from joint studies with NASA Ames Research Center, Aeronautics Division (through Agreements NCR-730-501 and NCA2-OR-730-601) and Grumman Aerospace Corporation, Research Department. We are pleased to acknowledge the advice and help on the use of FLO 22 code by R.M. Hicks, A. Levin, and R. Lasslo at the Ames Research Center. The senior author would like to thank G.L. Dwinell, C. Holguin, G. Karpouzian, and L. Murillo for their assistance in preparing the manuscript.

REFERENCES

1. Buseman, A. "Aerodynamischer Auftrieb bei Überschallgesch Windigkeit", Luftfuhrtforschung Bd. 12, Nr. 6, 1975, pp. 210-220.

2. Jones, R.T. "Wing Planform for High Speed Flight", NASA Report 863, 1945.

3. Jones, R.T. and Cohen, D. "Aerodynamics of Wings at High Speed", in Aerodynamic Components of Aircraft at High Speed, ed. by D.F. Donovan and H.R. Lawrence, Princeton University Press, 1957.

4. Kücheman, N.D. "Aerodynamic Design", The Aeronautical Journal, vol. 73, 1969, p. 101.

5. Jones, R.T. "Reduction of Wave Drag by Antisymmetric Arrangement of Wings and Bodies", AIAA Journal, vol. 10, Feb. 1972, pp. 171-176.

6. Bauer, F., Garabedian, P.R., Korn, D.G., and Jameson, A., Supercritical Wing Section, Springer-Verlag, Berlin, 1973.

7. Nieuland, G.Y. and Spee, B.M. "Transonic Airfoils: Recent Developments in Theory, Experiment and Design", Annual Review of Fluid Mechanics, vol. 5, 1973, pp. 119-150.

8. Boerstoel, J.W. "A Transonic Hodograph Theory for Airfoil Design", National Aerospace Laboratory Report, NLRMP 74024 U, Amsterdam, Netherlands, September 1974.

9. Kacprzynski, J.J., Ohman, L.H., Garabedian, P.R., and Korn, D.G. "Analysis of the Flow Past a Shockless Lifting Airfoil in Design and Off-Design Conditions", National Research Council of Canada, Aeronautical Report LR-554, Ottawa, 1971.

10. Whitcomb, R.T. "Review of NASA Supercritical Airfoils", Proc. 9th International Congress on Aeronautical Sciences, Haifa, Israel, 1974

11. Jones, R.T. "The Oblique Wing--Aircraft Design for Transonic and Low Supersonic Speeds", Acta Aeronautica, vol. 4, January 1977, pp. 99-110.

12a. Cheng, H.K. "Lifting-Line Theory of Oblique Wings", AIAA Journal, vol. 16, no. 11, 1978, pp. 1211-1213.

12b. Cheng, H.K. "Theory of Oblique Wings of High Aspect Ratio", University of Southern California, School of Engineering, Department of Aerospace Engineering, Report USCAE 135, August 1978.

13. Cheng, H.K. and Meng, S.Y. "Lifting-Line Theory of Oblique Wings in Transonic Flows", AIAA Journal, vol. 17, no. 1, 1979, pp. 121-124.

14a. Cheng, H.K. and Meng, S.Y. "The Oblique Wing as a Lifting-Line Problem in Transonic Flow", to appear in the Journal of Fluid Mechanics.

14b. Cheng, H.K. and Meng, S.Y. "The Oblique Wing as a Lifting-Line Problem in Transonic Flow", University of Southern California, School of Engineering, Department of Aerospace Engineering, Report USCAE 136, May 1979. (74 pages).

15. Cook, L.P. and Cole, J.D. "Lifting-Line Theory for Transonic Flow", SIAM Journal of Applied Mathematics, vol. 35, September 1978, pp. 209-224.

16. Cook, L.P. "A Uniqueness Proof of a Transonic Flow Problem", Indiana University Math. Journal, vol. 27, no. 1, 1978.

17. Small, R.D. "Transonic Lifting-Line Theory--Numerical Procedure for Shock-Free Flows", AIAA Journal, vol. 16, 1978, pp. 632-634.

18. Cook, L.P. "Lifting-Line Theory for a Swept Wing at Transonic Speeds", Quarterly Applied Mathematics, July 1979, pp. 178-202.

19. Prandtl, L. "Tragflügel Theorie", Nachrichten d.k. Gesellschaft d. Wiss 24, Göttingen, Math-Phys Klass, 1918, pp. 451-477.

20. Bailey, F.R. and Ballhaus, W.F. "Comparison of Computed and Experimental Pressures for Transonic Flows About Isolated Wings and Wing-Fuselage Configurations", NASA SP-347, Part II, 1975, pp. 1213-1231.

21. Jameson, A. "Iterative Solution of Transonic Flows Over Airfoils and Wings, Including Flows at Mach 1", Comm. Pure Appl. Math., vol. 27, 1974, pp. 283-309.

22. Jameson, A. and Caughey, D.A. "Numerical Calculations of the Transonic Flow Past a Swept Wing", Courant Inst. Math, Sciences, ERDA Math. Computing Lab., Report COO-3077-140 June 1977.

23. Jameson, A. and Caughey, D.A. "A Finite Volume Method for Transonic Potential Flow Calculations", Proc. AIAA 3rd Computational Fluid Dynamics Conference, Albuquerque, New Mexico, June 27-28, 1977, pp. 35-54.

24. Caughey, D.A. and Jameson, A., "Numerical Calculations of Potential Flow About Wing-Body Combinations", AIAA Journal, vol. 17, no. 2, 1979, pp. 175-181.

25. Hafez, M.M., South, J., and Murman, E. "Artificial Compressibility Methods for Numerical Solutions of Transonic Full Potential Equations", AIAA Journal, vol. 17, no. 8, 1979, pp. 838-906.

26. Chapman, D. "Computational Aerodynamics Development and Outlook", AIAA paper 79-0129, Dryden Lecture in Research presented at the 17th Aerospace Sciences Meeting, New Orleans, LA., January 15-17, 1979.

27. Van Dyke, M.D. Perturbation Methods in Fluid Mechanics, Acad. Press, New York, 1964, pp. 167-176.

28. Weisinger, J. "Ueber die Auftriebsverteilung von Pfeilflügeln", FB 1553, Berlin-Adlershof, 1942, NACA TM 1120, 1947.

29. Mutterperl, W. "The Calculation of Span Load Distribution on Swept-Back Wings", NACA TN 934, 1941.

30. Falkner, V.M. "Calculated Loadings Due to Incidence of a Number of Straight and Swept-Back Wings", Aeronautical Research Council, Report Memo 2596, 1948.

31. Hedman, S.G. "Vortex Lattic Method for Calculation of Quasi-Steady State Loadings on Thin Elastic Wings", Aeronautical Research Institute Sweden Report 105, October 1965.

32. Albano, E. and Rodden, W. "A Doublet-Lattice Method for Calculating Lift Distributions on Oscillating Surfaces in Subsonic Flows", AIAA Journal, vol. 7, no. 2, 1969, pp. 279-285.

33. Krienes, K. "The Elliptic Wing Based on the Potential Theory", ZAMM, vol. 20, no. 2, 1939, pp. 65-88; NACA Tech. Memo 97, 1940.

34. Doroditsyn, A.A. "Generalization of the Lifting-Line Theory for Cases of a Wing with a Curved Axis and a Slipping Wing", Prikl. Math. Mech., vol. 8, 1944, pp. 33-64.

35. Thurber, J. "An Asymptotic Method for Determining the Lift-Line Distribution on a Swept-Back Wing of Finite Span", Comm. Pure Appl. Math., vol. 18, 1965, pp. 733-750.

36. Cheng, H.K. "On Lifting-Line Theory in Unsteady Aerodynamics", University of Southern California, School of Engineering, Department of Aerospace Engineering Report USCAE 133, 1976.

37. Van Dyke, M.D. "Lifting-Line Theory as a Singular Perturbation Problem", Arch. Mech. Stos., vol. 16, no. 3, 1964, pp. 601-614, Appl. Math. Mech., vol. 28, 1964, pp. 90-101.

38. Kida, T. and Miyai, T. "An Alternative Treatment of Lifting-Line Theory as a Perturbation Problem", ZAMP, vol. 29, Fasc. 4, 1978, pp. 591-607.

39. Jones, R.T. "The Spanwise Distribution of Lift for Minimum Induced Drag of Wings Having a Given Lift and a Given Bending Moment", NACA Tech. Note 2249, 1950.

40. von Kármán, T. "The Similarity Law of Transonic Flow", Journal of Math. Phys., vol. 26, 1947, pp. 182-190.

41. Guderley, K.G. The Theory of Transonic Flow, Pergamon Press, London, 1962.

42. Spreiter, J.R. and Alksne, A. "Thin Airfoil Theory Based on Approximate Solutions of the Transonic Flow Equation", NACA Report 1359, 1958.

43. Murman, E.M. and Cole, J.D. "Calculation of Plane Steady Transonic Flows", AIAA Journal, vol. 9, no. 1, 1971, pp. 114-121.

44. Cole, J.D. "Modern Development in Transonic Flows", SIAM Journal Appl. Math., vol. 29, no. 4, December 1975, pp. 763-787.

45. Murman, E.M. and Krupp, "Solutions of the Transonic Potential Equation Using a Mixed Finite Difference System", Proc. 2nd International Conference on Numerical Methods in Fluid Dynamics, Lecture Notes in Physics, Springer-Verlag, Berlin-Heidelberg, New York, 1971, pp. 199-206.

46. Ballhaus, W.F. "Some Recent Progress in Transonic Flow Computations", text presented at the Lecture Series on Computational Fluid, von Kármán Institute, Rhode-St.-Genese, Belgium, March 15-19, 1976.

47. Courant, R. and Hilbert, D. Methods of Mathematical Physics, vol. II, 1965, pp. 551-556.

48. Landahl, M. "Linearized Theory for Unsteady Transonic Flow", in Symposium Transsonium, 1962, pp. 414-439.

49. Ballhaus, W.F. and Goorjians, P.M. "Implicit Finite Difference Computations of Unsteady Transonic Flows About Airfoils, Including the Treatment of Irregular Shock Wave Motions", AIAA Journal, vol. 15, no. 12, 1977, pp. 1728-1735.

50. Ferrari, A. and Tricomi, F.G. Transonic Aerodynamics, Academic Press, New York.

51. Manwell, A. Hodograph Equations: An Introduction to the Theory of Plane Transonic Flow, University Math. Monograph, no. 8. Edinburgh.

52. Morawetz, C.S. "On the Non-Existence of Continuous Transonic Flow Past Profiles, I, II, and III", Comm. Pure Appliec Math., vol. 9, 1956, pp. 45-68; vol. 10, 1957, pp. 107-131; vol. 11, 1958, pp. 129-144.

53. Nonweiler, T.R.F. "The Sonic Flow About Some Symmetric Half Bodies", Journal of Fluid Mechanics, vol. 4, pt. 2, 1958, pp. 140-148.

54. Cole, J.D. "Twenty Years of Transonic Flow", Boeing Scientific Res. Lab Doc. D1-82-0878, 1969.

55. Keyfitz, B.L., Melnik, R.E. and Grossman, B. "An Analysis of the Leading-Edge Singularity in Transonic Small and Disturbance Theory", Quart. Journal Mech. Appl. Math., vol. 31, pt. 2, May 1978, pp. 137-155.

56. Cheng, H.K., Chow, R. and Melnik, R.E. "Lifting-Line Theory of Swept Wings Based on the Full Potential Theory", (Draft of Report).

57. Oswatitsch, K. and Zierep, J. "Des Problem des Senkrechten Stossen and Einer Gekrummten Wand", ZAMM, vol. 40, Suppl. 1960, pp. 143-144.

58. Henne, P.A. and Hicks, R.M. "Transonic Wing Analysis Using Advanced Computational Methods", Douglas Aircraft Co., McDonnell Douglas Corp., Douglas Paper 6647.

59. Murman, E.M. "Analysis of Embedded Shock Waves Calculated by Relaxation Methods", AIAA Journal, vol. 12, 1974, pp. 626-633.

60. Meng, S.Y. and Cheng, H.K. "Convergence Acceleration of Relaxation Solutions by the Power Method: Higher-Order Algorithms", Proc. Appl. Computer Methods in Engineering, held at the University of Southern California, Los Angeles, ed. L.C. Wellford, 1977, pp. 395-404.

61. Hafez, M.M. and Cheng, H.K. "Shock-Fitting Applied to Relaxation Solutions of Transonic Small-Disturbance Equations", AIAA Journal, vol. 15, no. 6, 1977, pp. 786-793.

62. Black, R.L., Beamish, J.K. and Alexander, W.K. "Wind Tunnel Investigation of an Oblique Wing Transport Model at Mach Number Between 0.6 and 1.4", NASA CR-137 697, HST-TR-344-C, July 1975.

FIGURE CAPTIONS

Fig. 1 The bound and trailing vortex system illustrated for (a) a pivoted (oblique) straight wing, (b) swept wingswith straight center-line segments, and (c) swept wings with curved center line.

Fig. 2 The Cartesian and the orthogonal curvilinear coordinates illustrated for the wing plane. The ξ and η-ordinates are normal to the wing plane.

Fig. 3 Illustration of a spanwise component of the trailing vorticity which induces to a logarithmically infinite upwash.

Fig. 4 The upwash function $\bar{\Sigma}$ illustrated for $A_R = 8.39$ at three yaw angles for an elliptic and an extended-span distribution in $\bar{\Gamma}_0$.

Fig. 5 The upwash function $\bar{\Sigma}_0$, $\bar{\Sigma}_0^c$ illustrated for elliptically loaded swept-forward and swept-back wings of $A_R = 14$ at $M_\infty = 0.755$. Refer to text for conversion to other aspect ratio and Mach numbers.

Fig. 6 Sketches illustrating different types of wing tip geometry: (a) elliptic or parabolic type, (b) tapered swept-wing (standard) (c) tapered swept wing.

Fig. 7 Spanwise Distribution of sectional lift coefficient computed for an oblique wing by solutions to the full potential equation (FLO 22) from two sources.

Fig. 8 Similarity solutions for $\bar{\Gamma}_{0\bar{x}}$, $\bar{\beta}_{1,\bar{x}}$, and $\bar{\beta}_{2\bar{x}}$ on the upper and lower surfaces of an oblique wing at $M_n = 3.45$. The straight axis is located at the mid chord; the airfoil section is generated from NASA 3612-02,40 rescaled to an arbitrary thickness; the section is set at zero incidence, without twist and without wing bend.

Fig. 9 A consolidated plot showing surface C_p on three span stations of a high-aspect-ratio wing pivoted at 22.5°, at Flight Mach number 0.824. The planform is a 20:1 ellipse; the wing section is NASA 3606-02,40 set at zero incidence, without twist and without bend.

Fig. 10 A consolidated plot showing surface C_p on seven span stations of an oblique wing pivoted at 30°, at Flight Mach number 0.767. The planform is a 14:1 ellipse; the wing section is NASA 3612-02,40, zero incidence, zero twist and zero wind bend.

Fig. 11 A consolidated plot showing surface C_p on seven span stations of a symmetric swept-back wing with 30° sweep angle, at Flight Mach number of 0.755. The basic planform is a 14:1 ellipse; the wing section is NASA 3612-02,40, zero incidence, zero twist and no wing bend.

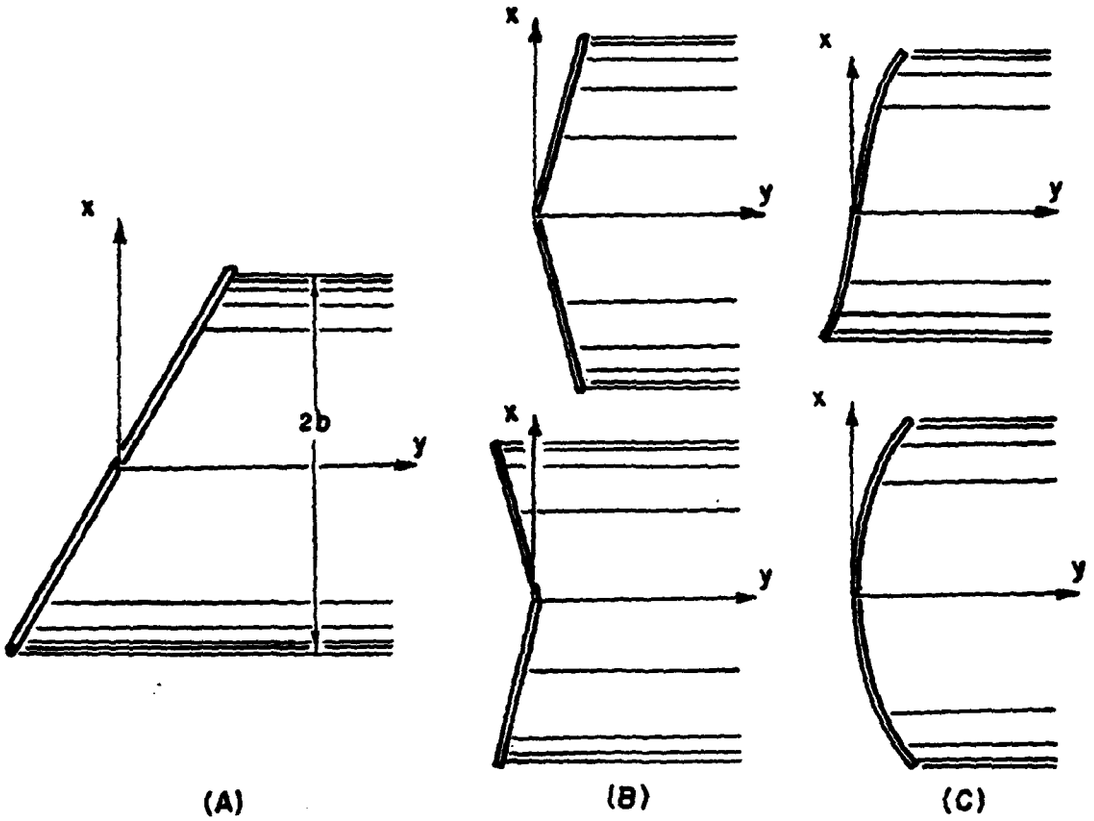

Figure 1

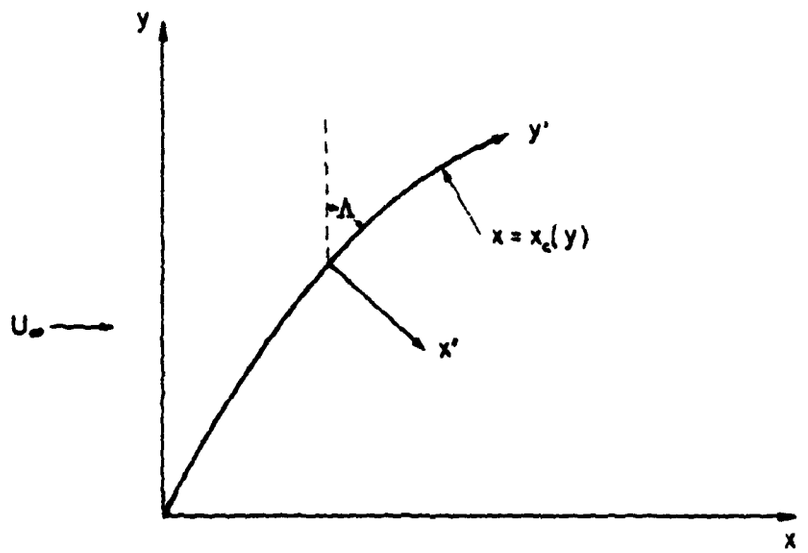

Figure 2

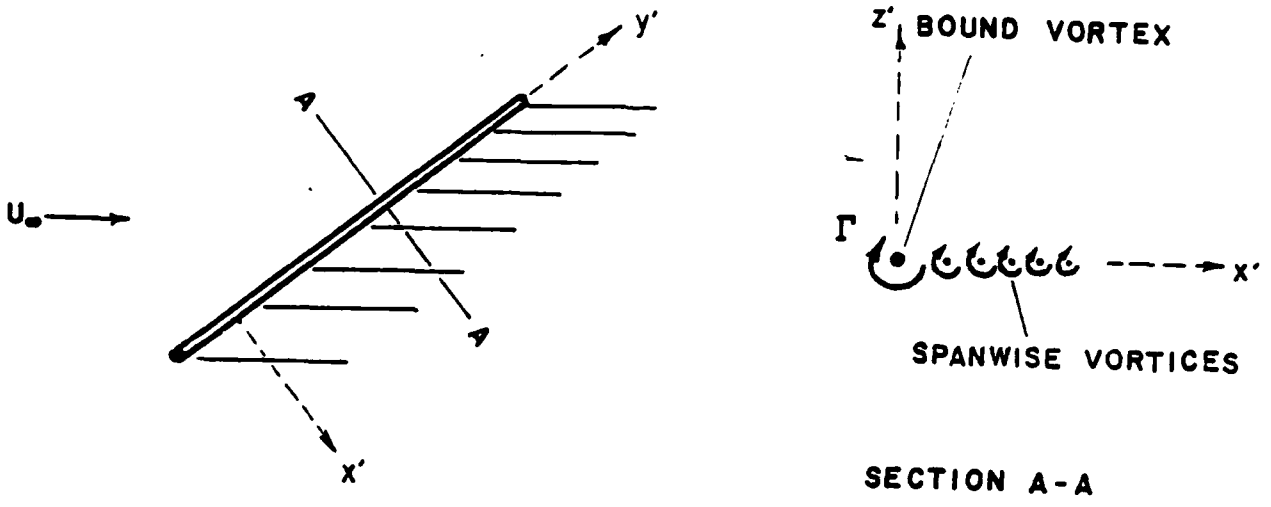

Figure 3

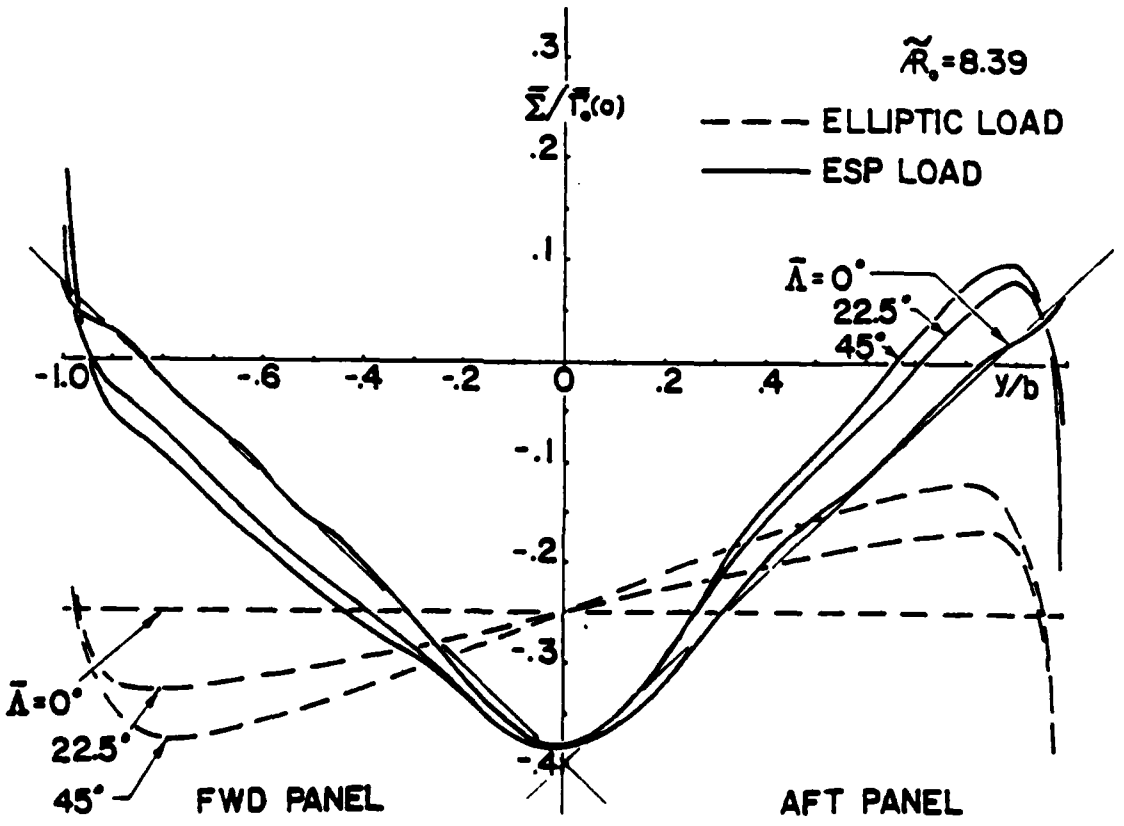

Figure 4

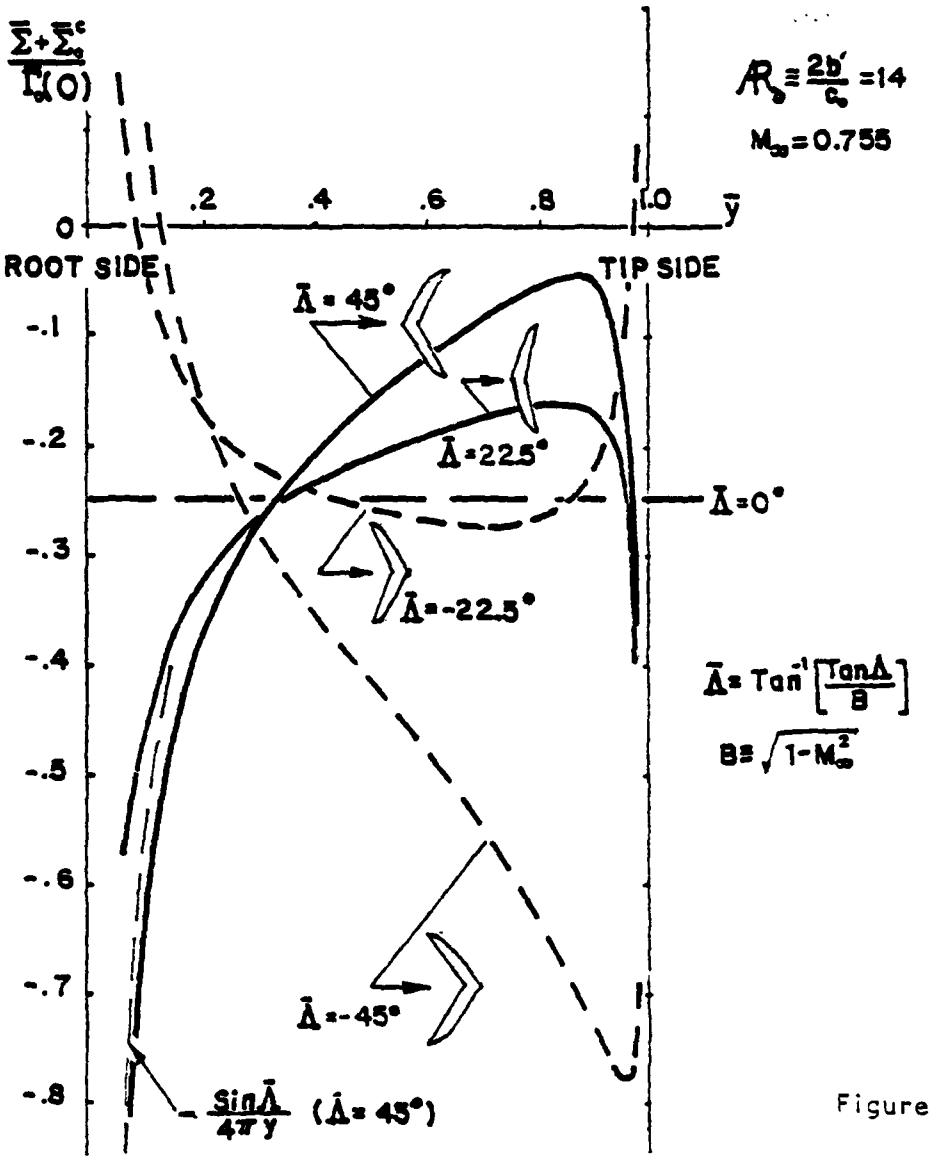

Figure 5

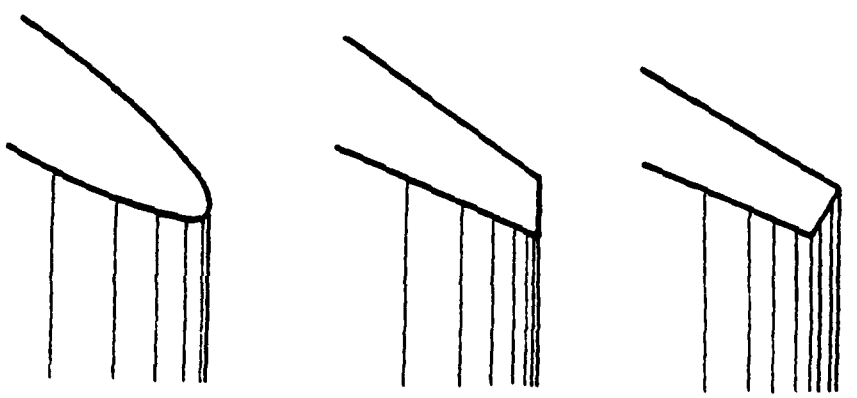

(A) (B) (C)

Figure 6

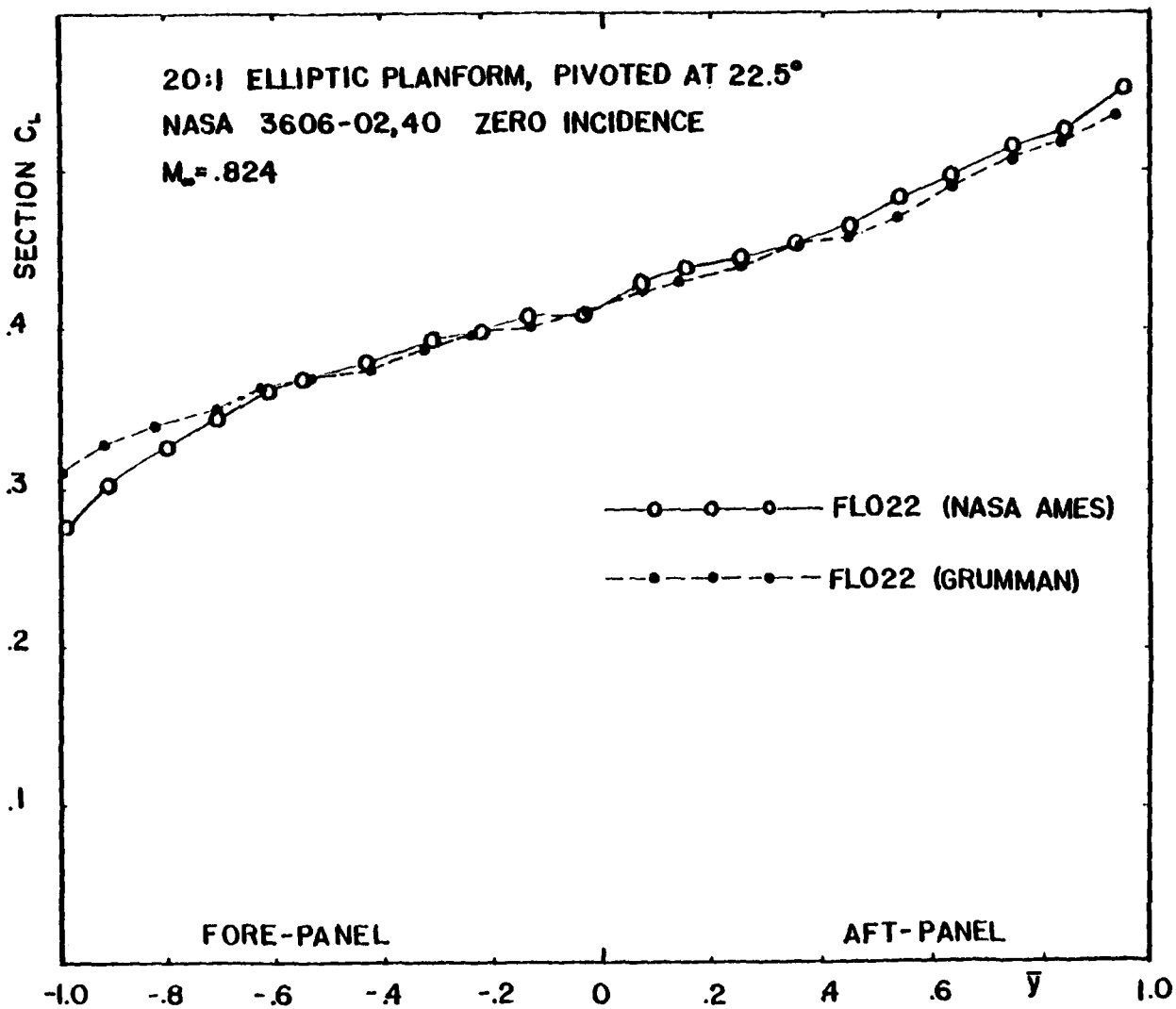
20:1 ELLIPTIC PLANFORM, PIVOTED AT 22.5°
NASA 3606-02,40 ZERO INCIDENCE
M∞=.824
SECTION C_L
.4
.3
.2
.1
FLO22 (NASA AMES)
FLO22 (GRUMMAN)
FORE-PANEL
AFT-PANEL
-1.0
-.8
-.6
-.4
-.2
0
.2
.4
.6
ȳ
1.0

Figure 7

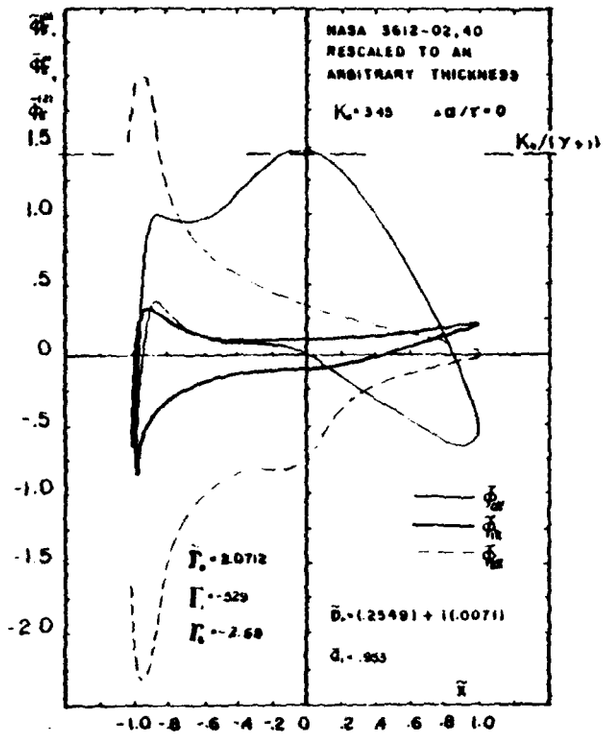

Figure 8

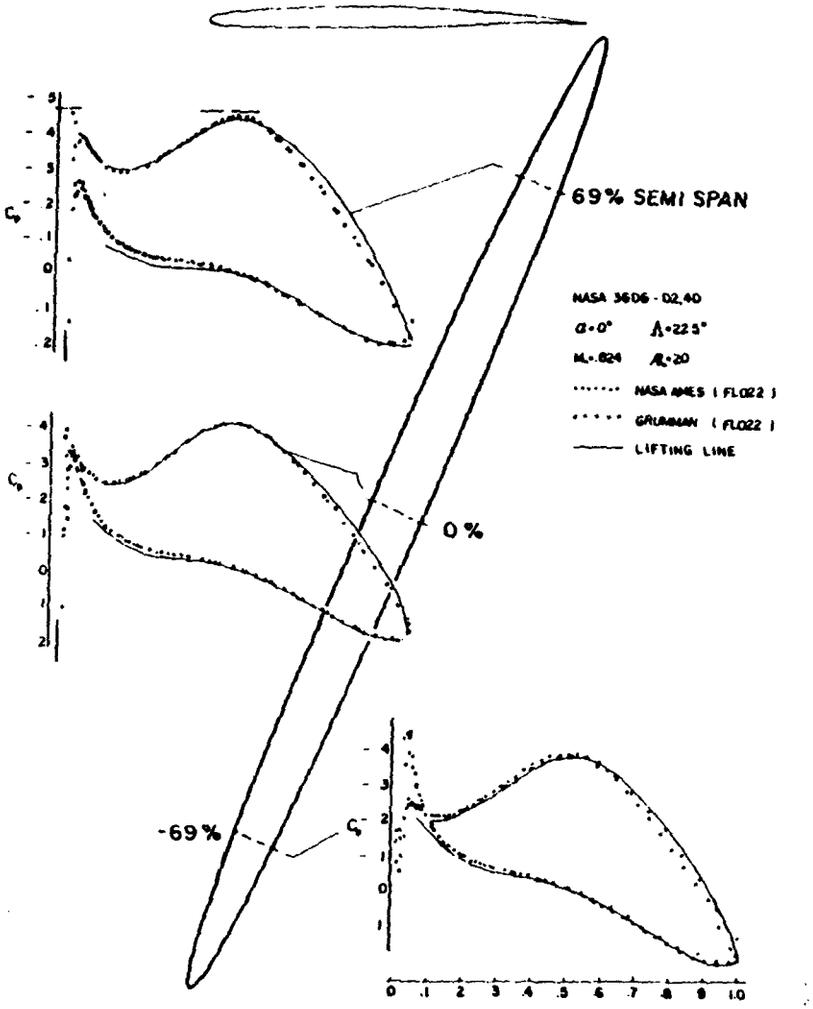

Figure 9

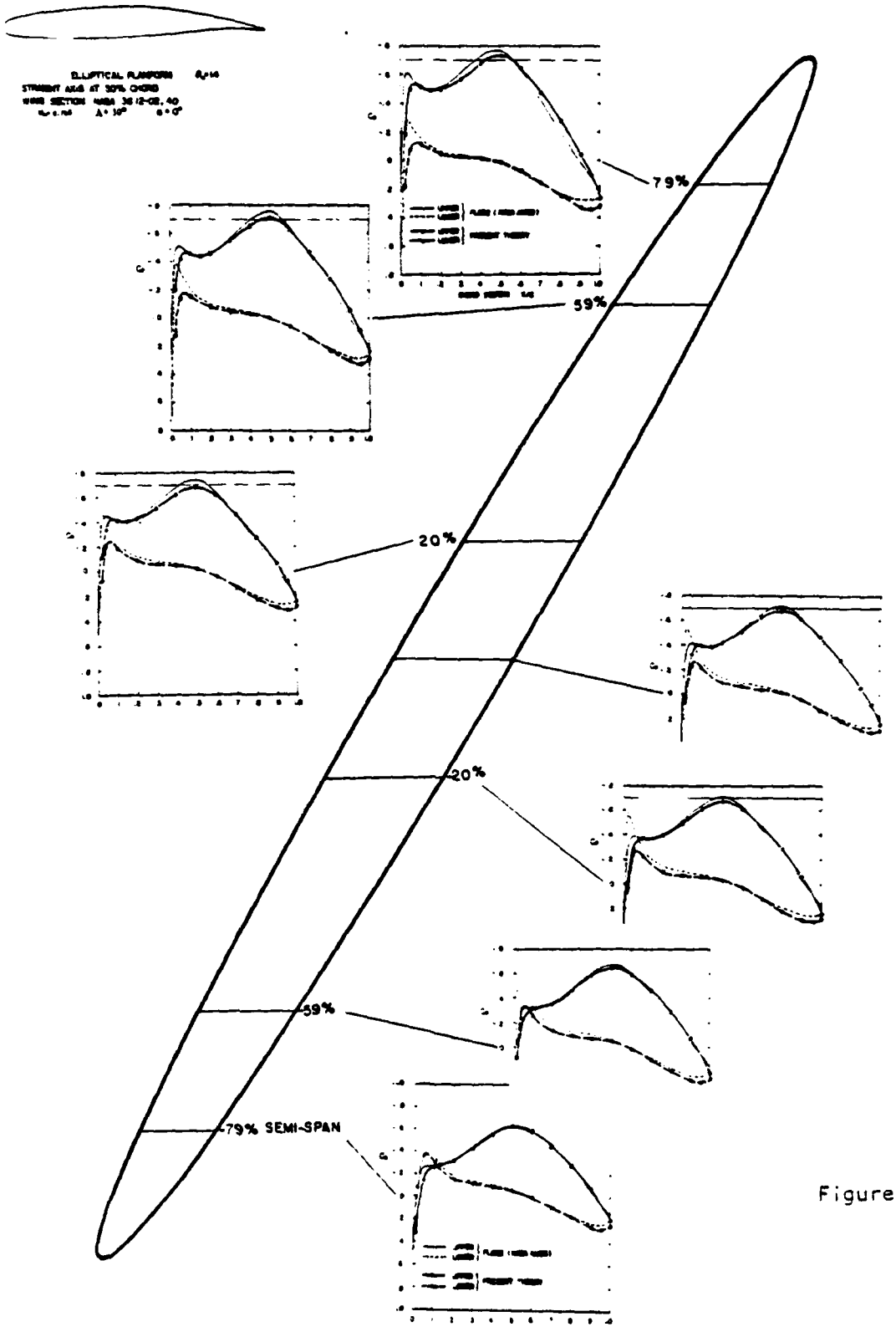

Figure 10

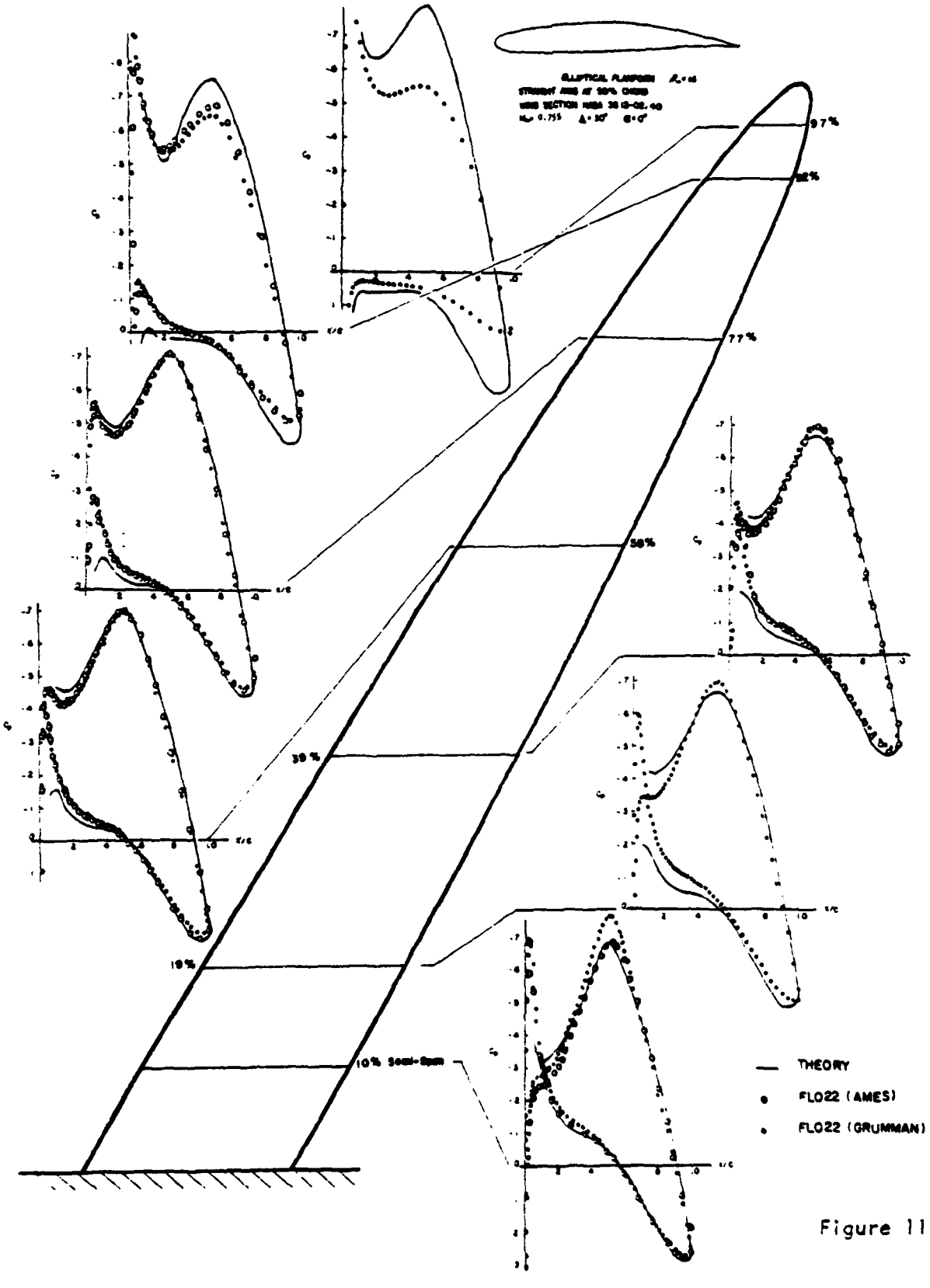

Figure 11

UNCLASSIFIED
SECURITY CLASSIFICATION OF THIS PAGE *(When Data Entered)*

REPORT DOCUMENTATION PAGE		READ INSTRUCTIONS BEFORE COMPLETING FORM
1. REPORT NUMBER	2. GOVT ACCESSION NO. AD-A085587	3. RECIPIENT'S CATALOG NUMBER
4. TITLE *(and Subtitle)* Transonic Swept-Wing Analysis Using Asymptotic and Other Numerical Method		5. TYPE OF REPORT & PERIOD COVERED Technical Report
		6. PERFORMING ORG. REPORT NUMBER
7. AUTHOR(s) H. K. Cheng, S. Y. Meng, R. Chow and R. Smith		8. CONTRACT OR GRANT NUMBER(s) ✓N00014-75-C-0520
9. PERFORMING ORGANIZATION NAME AND ADDRESS University of Southern California Department of Aerospace Engineering ✓ Los Angeles, California 90007		10. PROGRAM ELEMENT, PROJECT, TASK AREA & WORK UNIT NUMBERS
11. CONTROLLING OFFICE NAME AND ADDRESS Department of the Navy, Code 438 Office of Naval Research Arlington, Virginia 22217		12. REPORT DATE April 1980
		13. NUMBER OF PAGES
14. MONITORING AGENCY NAME & ADDRESS(if different from Controlling Office) Department of the Navy, Code 603 Office of Naval Research, Branch Office 1030 East Green Street Pasadena, California 91106		15. SECURITY CLASS. (of this report) Unclassified
		15a. DECLASSIFICATION/DOWNGRADING SCHEDULE

16. DISTRIBUTION STATEMENT *(of this Report)*

"Approved for public release; distribution unlimited".

17. DISTRIBUTION STATEMENT *(of the abstract entered in Block 20, if different from Report)*

18. SUPPLEMENTARY NOTES

19. KEY WORDS *(Continue on reverse side if necessary and identify by block number)*

Swept wing
Oblique wing
Swept forward wing
Transonic flow
Comparison with full-potential solution
Asymptotic theory
Similarity solutions

20. ABSTRACT *(Continue on reverse side if necessary and identify by block number)*

Asymptotic theories for high-aspect-ratio wings in transonic flow developed recently show that the three-dimensional (3-D) mixed-flow calculations may be reduced to solving a set of 2-D problems at each span station. For wings with surfaces generated from a single airfoil shape, local similitude exists in the 3-D flow structure, permitting the problems to be solved once for all span stations. This paper reviews this theoretical development. The essential elements in the theory will be identified. Their relationship to the lifting-line theory and related classical methods are discussed. (cont.)

DD FORM 1 JAN 73 1473

UNCLASSIFIED
SECURITY CLASSIFICATION OF THIS PAGE *(When Data Entered)*

20 cont.

Examples of similarity solutions are demonstrated for high subcritical and slightly super-critical component flows; comparisons with relaxation solutions to a full potential equation are made. The study also examines the adequacy of the existing full-potential computer code. Outstanding problems remaining for subsequent development are discussed.

USG
Engineering